ABSTRACT

Title of Thesis: EXCITATION-CONTRACTION COUPLING DISRUPTION IN A MOUSE MODEL OF NIEMANN-PICK DISEASE

Harry Zichen Li, Master of Arts, 2017

Directed By: Dr. Eva Chin, PhD, Department of Kinesiology

Niemann-Pick disease (NPD) is a lysosomal storage disorder that results from deficient acid sphingomyelinase (ASM) activity. It was recently proposed that ASM and extracellular Ca^{2+} are required for membrane repair. Since plasma membrane integrity is an important component of excitation-contraction coupling (E-C) and skeletal muscle force production, we hypothesized that there would be E-C coupling defects in NPD related to intracellular calcium (Ca^{2+}) dynamics. Our results demonstrate that ASM deficient (ASM-/-) fibers have a reduced ability to withstand repetitive contractions in comparison to wild-type (WT) fibers, and fibers from ASM-/- mice exhibited lower peak tetanic Ca^{2+} compared to WT. Lastly, no differences in peak tetanic Ca^{2+} were found between ASM-/- fibers and WT fibers deprived of Ca^{2+}. Together, these results suggest that both ASM and extracellular Ca^{2+} are required for optimal E-C coupling in skeletal muscle and for the ability to respond to repetitive contractions that occurs with sustained activity.

EXCITATION-CONTRACTION COUPLING DISRUPTION IN A MOUSE MODEL OF NIEMANN-PICK DISEASE

By

Harry Zichen Li

Thesis submitted to the Faculty of the Graduate School of the
University of Maryland, College Park, in partial fulfillment of the
requirements for the degree of
Master of Arts
2017

Advisory Committee:
Dr. James Hagberg, Chair; Professor, Kinesiology
Dr. Eva Chin, Adjunct Professor, Kinesiology
Dr. Norma Andrews, Professor, Cell Biology and Molecular Genetics

Acknowledgements

I would like to express my sincere gratitude to my advisor, Dr. Eva Chin, and to my committee members, Dr. James Hagberg and Dr. Norma Andrews, for their guidance, expertise, and immense patience.

I am indebted to Dr. Davi Mázala, Mr. Daniel Shill, and Mr. Ber-an Pan for their support, words of encouragement, and assistance in preparing this manuscript.

I am grateful to Dr. Vladimir Ribeiro, Dr. Fernando Maeda, and Dr. Maria da Silva for their flexibility and cooperation with sample preparation.

I would also like to thank Dr. Sarah Glancy for her patience and encouragement on this project.

Finally, I would like to acknowledge the University of Maryland's Department of Kinesiology for supporting my research through the Graduate Student Research Initiative Fund.

Table of Contents

List of Abbreviations

ACh - Acetylcholine
ADP – Adenosine diphosphate
ASM – Acid sphingomyelinase
ASM-/- – Acid sphingomyelinase knockout
ATP – Adenosine triphosphate
AM – Acetoxymethyl
ANOVA - Analysis of variance
BEL – Bromoenol lactone
BFA – Brefeldin A
Ca^{2+} – Calcium
$[Ca^{2+}]_i$ – Intracellular calcium concentration
$CaCl_2$ – Calcium chloride
CARF – Central animal research facility
Cav1 – Caveolin-1
Cav3 – Caveolin-3
CMNS – College of Computer, Mathematical, and Natural Sciences
CO_2 – Carbon dioxide
Cr – Creatine
CrP – Creatine phosphate
DHPR – Dihydropyridine receptors
DMD – Duchenne muscular dystrophy
DPA – Desipramine
E-C – Excitation-contraction
EDL – Extensor digitorum longus
FBS – Fetal bovine serum
FDB – Flexor digitorum brevis
GFP – Green fluorescent protein
H^+ – Hydrogen ion
Hz – Hertz
IACUC – Institutional Animal Care and Use Committee
KCl – Potassium cloride
MEM – Minimal essential media
Mg^{2+} – Magnesium
$MgCl_2$ – Magnesium chloride
NaCl – Sodium chloride
$NaHCO_3$ – Sodium bicarbonate
NaH_2PO_4 – Sodium phosphate
NPD – Niemann-Pick disease
NPD/A – Niemann-Pick disease type A
NPD/B – Niemann-Pick disease type B
NPD/C – Niemann-Pick disease type C
NRK – Normal rat kidney epithelial
O_2 – Oxygen

PI – Propidium iodide
Pi – Inorganic phosphate
PKC – Protein kinase C
RTC – Repeated tetanic contraction
RyR – Ryanodine receptor
SE – Standard error
SERCA – Sarcoplasmic/endoplasmic reticulum calcium ATPase
SLO – Streptolysin O
SMF – Single muscle fiber
SR – Sarcoplasmic reticulum
SSM – Secretory sphingomyelinase
Syt – Synaptotagmin
WT – Wild type
Zn^{2+} – Zinc

List of Tables

List of Figures

Chapter 1: Introduction

Patients with Niemann-Pick disease (NPD) type A or type B have an inherited deficiency of acid sphingomyelinase (ASM). This disorder occurs in ~1 in every 250,000 births (Meikle, Hopwood, Clague, & Carey, 1999). There is a wide range of phenotypes for ASM deficiency in that patients with type A NPD (NPD/A) develop symptoms within the first 6 months of life while patients with type B NPD (NPD/B) express milder symptoms during mid-childhood to teenage years. These symptoms may include neurodegeneration (Mendelson et al., 2006), hepatosplenomegaly (i.e. enlarged liver and spleen), pulmonary infections, and, most relevantly, hypotonia (i.e. muscle weakness) (Gumbinas, Larsen, and Liu, 1975; Horinouchi et al., 1995).

Acid sphingomyelinase (ASM) is a lysosomal enzyme that hydrolyzes sphingomyelin into ceramide and phosphorylcholine (Kanfer et al., 1966), and is particularly important in calcium (Ca^{2+})-triggered cell membrane repair (Corrotte et al., 2013). Briefly, after cells are wounded, extracellular Ca^{2+} enters the cell and triggers a repair mechanism to rapidly reseal the plasma membrane (McNeil, Miyake, & Vogel, 2003). There are two major proposed mechanisms for plasma membrane repair in the literature. One hypothesis states that a membrane patch is formed to cover the wound site (Miyake & McNeil, 1995), while another hypothesis suggests that membranes are resealed through the reduction in membrane tension via exocytosis (Togo, Krasieva, & Steinhardt, 2000).

Although previous proposed mechanisms for plasma membrane repair can sufficiently explain repairs of mechanical wounds on membranes, such mechanisms are unable to explain how membrane repair occurs when compromised by pore-forming toxins. Corrotte and colleagues (2013) suggested a new mechanism of caveolae internalization to explain such repairs. In brief, Corrotte and colleagues (2013) suggested that Ca^{2+}-triggered release of sphingomyelinase induces endocytosis and accumulation of caveolar vesicles. During mechanical wounding, these vesicles subsequently fuse into larger caveolae while drawing the edge of the wound closer together, resulting in the resealing of the membrane (Figure 1). However, when exposed to pore-forming toxins, caveolae internalization is able to repair the plasma membrane by forming individual caveolae around the toxins, removing them from the plasma membrane, and transporting them internally for disposal (Figure 2; Corrotte et al., 2013).

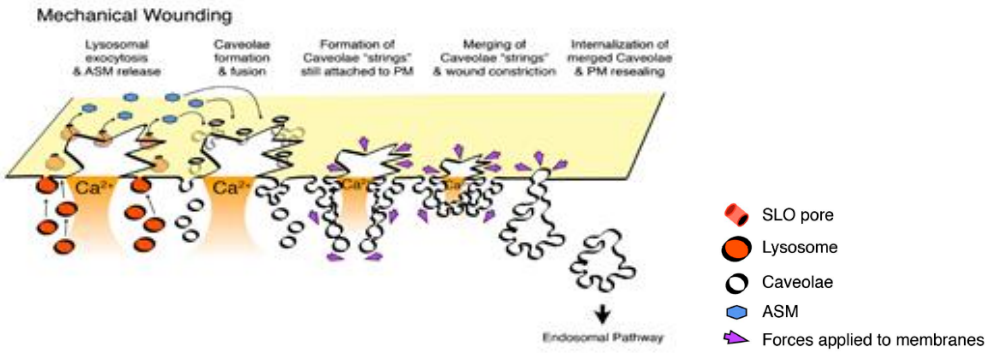

Figure 1. Mechanism of membrane repair after mechanical wounding. Mechanical wounding allows the influx of Ca^{2+}, triggering the exocytosis of lysosomes (orange circles), which release ASM (blue hexagons), that promote the formation and internalization of caveolae (white circles). Caveolae then cluster and fuse to draw the wound closed. Adapted from Corrotte et al. (2013).

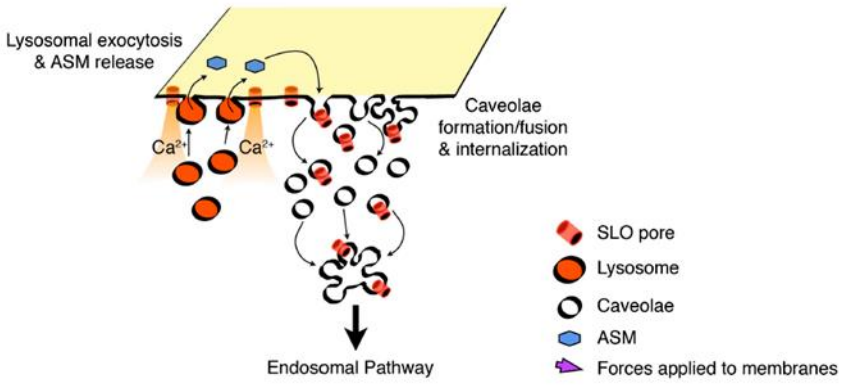

Figure 2. Mechanism of membrane repair in response to pore-forming toxins. Pore-forming toxins allow the influx of Ca^{2+}, triggering the exocytosis of lysosomes (orange circles), which release ASM (blue hexagons), that initiate the formation and internalization of caveolae (white circles). Individual caveolae remove the toxins (small orange rectangles) from the membrane, thus removing the pore and resealing the area. Adapted from Corrotte et al. (2013).

Only a limited number of studies have evaluated the role of NPD and ASM deficiency with respect to skeletal muscle function. McGovern et al. (2008) found impaired pulmonary gas exchange in patients with NPD/B using maximal exercise tolerance testing. Macauley, Sidman, and Schuchman (2008) performed rotarod tests on ASM deficient (ASM-/-) mice and found that performance deteriorated after 7 weeks of age. Although Corrotte and colleagues (2013) did not evaluate the role of NPD and ASM deficiency and their impact on skeletal muscle function, their study did explore the role of ASM in skeletal muscle membrane repair. Specifically, they evaluated caveolae internalization and plasma membrane repair in single muscle fibers from the mouse flexor digitorum brevis (FDB) muscle (Corrotte et al., 2013). Their findings showed that without ASM, muscle membrane repair was reduced, implicating a requirement for ASM in muscle membrane repair. While their study did not address skeletal muscle function, their

investigation into plasma membrane repair and its impairments help lead to hypothesizing a mechanism for explaining the muscle weakness observed with NPD.

Notably, there is evidence to suggest that the plasma membranes of cells deficient in ASM are damaged or compromised (Butler et al., 2002). The lack of ASM leads to over accumulation of sphingomyelin in the plasma membrane and lysosomes of fibroblasts from ASM-/- mice (Gabandé-Rodriguez, 2014). This over accumulation contributes to the instability of the plasma membrane and lysosomes, which can lead to cytosolic leakage (Gabandé-Rodriguez, 2014). Additionally, the spermatozoa of these ASM-/- mice showed an overabundance of sphingomyelin in their plasma membranes, and only 13.4% of the spermatozoa showed intact plasma membranes (Butler et al., 2002). Similarly, approximately 50% of isolated single muscle fibers from ASM-/- mice exhibited evidence of membrane injury (Andrews, personal communication).

Notwithstanding, plasma membrane integrity is a critical component of the excitation-contraction (E-C) coupling and muscle force production. Skeletal muscle activation begins with an action potential from a motor neuron that releases acetylcholine (ACh) into the synaptic cleft of the neuromuscular junction. The ACh binds to ACh receptors located on the motor end plate of the sarcolemma causing sodium (Na^+) channels to open and allow the influx of Na^+. This change in electrochemical gradient depolarizes and propagates across the sarcolemma before traveling down invaginations of the plasma membrane, i.e. T-tubules, to activate voltage-gated dihydropyridine receptors (DHPR). The DHPRs cause a conformational change in the ryanodine receptors (RyR) to allow the efflux of Ca^{2+} from the sarcoplasmic reticulum (SR). The released Ca^{2+} then binds to troponin, allowing troponin to move tropomyosin away from the myosin binding site

located on actin. Myosin is then able to bind to actin and form cross-bridges, which subsequently leads to sarcomere shortening and muscle fiber contraction (Ashley, Mulligan, & Lea, 1992; Figure 3). Alterations in the E-C coupling pathway, particularly at or before the activation of DHPRs, may change Ca^{2+} kinetics thus leading to impaired muscle contraction and force production (Lamb, 2009).

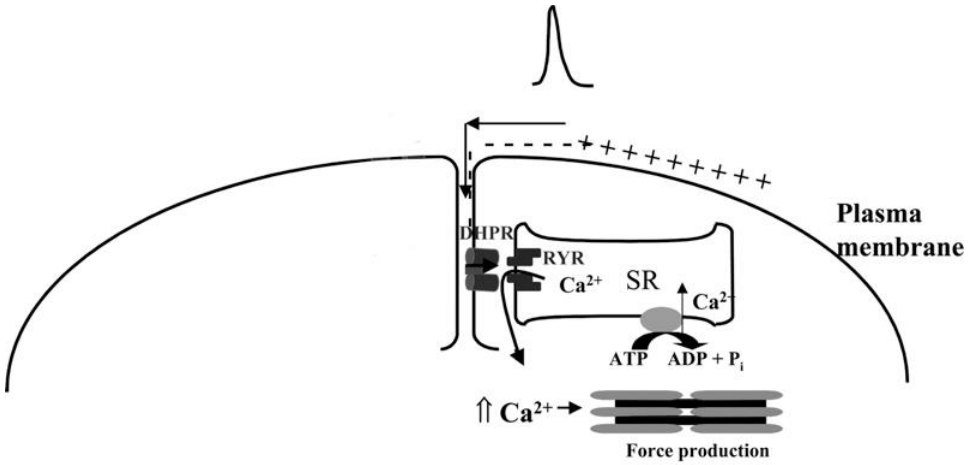

Figure 3. Excitation-contraction coupling. Activated motor neurons release acetylcholine resulting in the opening of Na^+ channels and depolarization, which propagates across the sarcolemma and down the T-tubules to activate the DHPR. Activated DHPR causes a conformational change in RyR to release Ca^{2+} from the SR. Ca^{2+} binds to troponin to move tropomyosin, thereby freeing the myosin binding site on actin. Myosin then binds to actin to initiate cross-bridge cycling, which results in muscular contraction and force production. Adapted from Chin (2005).

Several studies have demonstrated that muscle fatigue transpires as a result of impairments in the process of E-C coupling (Allen, Lee, & Westerblad, 1989; Chin & Allen, 1995; Westerblad & Allen, 1991). A decrease in free intracellular Ca^{2+} concentration ($[Ca^{2+}]_i$) and force production during repeated tetanic contractions is a result of E-C coupling impairment, which can be due to both metabolite accumulation and to the

elevations in $[Ca^{2+}]_i$-time integral (Chin, Balnave, & Allen, 1997). Other possible causes for the impairments in E-C coupling and force production include deficiencies in depolarization, slower membrane repolarization, DHPR activation failure, communication impairment between DHPR and the RyR, and decline in Ca^{2+} uptake rate into the SR (Lamb, 2009). Prolonged effects of muscle fatigue persisting after metabolic recovery, which can manifest as muscle weakness, are thought to be due solely to the increases in $[Ca^{2+}]_i$ during the tetanic contractions (Chin & Allen, 1995). The accumulation of $[Ca^{2+}]_i$ during repeated tetanic contractions may also be responsible for the reduced force production capacity observed in some muscle diseases (Lamb, Junankar, & Stephenson, 1995; Verburg, Dutka, & Lamb, 2006), and may play a role in NPD.

There may be a link between the impaired membrane repair mechanism and E-C uncoupling in ASM-/- fibers. In ASM-/- fibers, ASM deficiency prevents caveolae formation, thereby leaving the damaged membrane unrepaired (Corrotte et al., 2013). Similarly, when wounded cells recover in the presence of EGTA, which chelates extracellular Ca^{2+}, exocytosis of lysosomes and membrane repair is inhibited (Reddy et al., 2001). Both ASM deficiency and lack of extracellular Ca^{2+} fail to trigger membrane repair. Given the observed membrane repair failure in both circumstances, we believe that that a compromised membrane is subsequently unable to fully propagate an electrical signal leading to diminished Ca^{2+} release.

E-C coupling may be disrupted in ASM-/- muscle fibers based on the evidence of poor membrane repair. Additionally, E-C uncoupling may be exacerbated through prolonged stimulation leading to muscle weakness in ASM-/- mice. Therefore, the purpose of the proposed study is three-fold: 1) to evaluate E-C coupling in single muscle fibers

from ASM-/- mice, as an indirect measure of muscle function; 2) to determine if E-C uncoupling is more prominent in muscle from ASM-/- compared to wild-type (WT) mice after repeated tetanic stimulation; and, 3) to evaluate the association between impaired membrane repair and E-C uncoupling by comparing ASM deficiency with Ca^{2+} deprivation.

Specific Aims

Specific aim 1 – To determine if E-C coupling is impaired in ASM-/- muscle fibers compared to WT fibers.

Hypothesis 1 – It is hypothesized that stimulation-induced peak Ca^{2+} transients are lower in single muscle fibers from ASM-/- mice compared to WT.

Specific aim 2 – To determine if E-C coupling disruption is more prominent in ASM-/- muscle fibers compared to WT muscle fibers after repeated tetanic contractions.

Hypothesis 2 – It is hypothesized that following repeated contractions WT muscle fibers will fully recover to their initial peak Ca^{2+} levels but ASM-/- muscle fibers will have a prolonged reduction of peak Ca^{2+} transients.

Specific aim 3 – To determine if extracellular Ca^{2+} and ASM are required for recovery from repeated tetanic contractions.

Hypothesis 3 – It is hypothesized that extracellular Ca^{2+} and ASM are both required for recovering of E-C coupling defects after repeated tetanic contractions. It is expected that intracellular Ca^{2+} transients will be reduced to a greater extent when single muscle fibers from ASM-/- mice recover in the absence of Ca^{2+}.

Chapter 2: Methods

2.1 – Animal handling and muscle fiber isolation

Six wild-type (WT) and six ASM-/- mice were used. The ASM-/- mice were acquired in collaboration from Dr. Norma Andrews in the College of Computer, Mathematical, and Natural Sciences (CMNS). Colonies of ASM-/- mice were kept and bred by Dr. Andrews's lab located at the University of Maryland. At about 8 weeks of age, the mice were used for assessment of E-C coupling in single muscle fibers. All protocols for animal handling have been approved by the Institutional Animal Care and Use Committee (IACUC). At the time of use, the mice were euthanized, and the FDB muscle was excised and digested in a type 2 collagenase/Minimal Essential Media (MEM)/Fetal Bovine Serum (FBS) solution at 37°C for four hours to acquire the FDB single muscle fibers (Chin et al. 2014; Mázala et al., 2015).

2.2 – Intracellular Ca^{2+} measurements

We used Fura-2AM to assess changes in intracellular Ca^{2+} levels in single muscle fibers. Briefly, after the single muscle fibers were isolated from the FDB muscle, the fibers were loaded with Fura-2AM for 15 minutes, which allows the fluorescent dye sufficient time to diffuse into the myoplasm. Fura-2 emits a signal when excited at 380nm (unbound state) or at 340nm (bound to Ca^{2+}), and the ratio at 340nm/380nm reflects the intracellular Ca^{2+} concentration ($[Ca^{2+}]_i$). The loaded fibers were then washed of excess dye and placed in a stimulation chamber containing parallel electrodes. The stimulation chamber was placed on top of a Nikon TiU microscope, and the IonOptix Hyperswitch system was used to assess the Fura-2 fluorescence ratio. Our lab has previously used this method to assess

E-C coupling defects in various mouse models of disease (Chin, Chen, Bobyk, & Mázala, 2014; Mázala et al., 2015).

2.2.1 – Single muscle fiber stimulation protocol

Single muscle fiber $[Ca^{2+}]_i$ was measured using 350msec tetani stimulated at 10, 30, 50, 70, 100, 120, and 150Hz frequencies. This was completed three times, at baseline (before) and 30 and 60 minutes after the repeated tetanic contraction protocol. The muscle fibers were allotted one minute of rest between each stimulation frequency, and five minutes of rest before the repeated tetanic contraction protocol. The muscle fibers were perfused with one of two stimulation solutions throughout the experiment. A Ca^{2+}-present stimulation solution was comprised of 121.0mM NaCl, 5.0mM KCl, 0.5mM $MgCl_2$, 0.4mM NaH_2PO_4, 24.0mM $NaHCO_3$, 5.5mM glucose, and 1.8mM $CaCl_2$ (Chin & Allen, 1998). To create a Ca^{2+}-absent stimulation solution, the 1.8mM $CaCl_2$ was replaced with 5mM EGTA, a Ca^{2+} chelating agent. Fetal bovine serum (FBS) (0.2%) was added to the stimulation solutions (Chin & Allen, 1998). The stimulation solution was continuously bubbled with 95% O_2/5% CO_2 and maintained at a pH of 7.3 (Chin & Allen, 1998).

After the first stimulation protocol and recovery period, the fibers were subjected to repeated tetanic contractions (RTC) by intermittent 100Hz stimulations (350msec duration). The fibers underwent one contraction every four seconds for two minutes, one contraction every three seconds for two minutes, one contraction every two seconds for two minutes, and finally one contraction every one second until peak Fura-2 ratio reduced to 50% of the initial ratio (Chin & Allen, 1995). This 50% decrease in peak Ca^{2+} transient level has been previously shown to correspond to a 70% decrease in force in isolated fibers

exposed to RTC, which was defined as the point of fatigue (Chin & Allen, 1996). At 30 and 60 minutes following RTC, $[Ca^{2+}]_i$ was assessed to determine the effects on E-C coupling and recovery. An overview of the protocol can be seen in Figure 4.

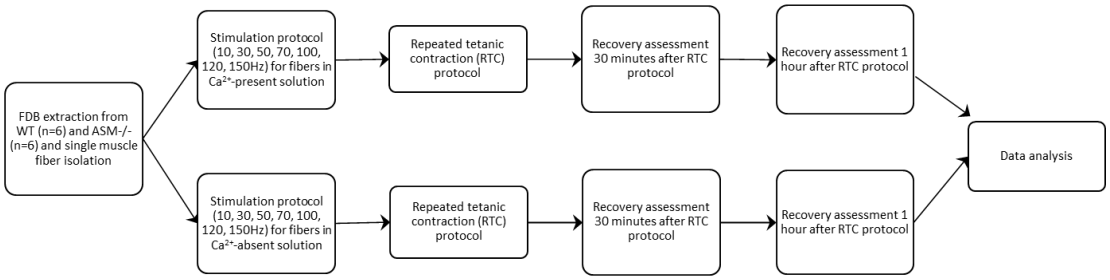

Figure 4. Schematic overview of protocol. FDB muscle was extracted from mice and digested with collagenase to isolate single muscle fibers. Stimulation protocol, repeated tetanic contraction protocol, and recovery assessment were performed on WT and ASM-/- in either Ca^{2+}-present or Ca^{2+}-absent stimulation solution. Data collected was then analyzed.

2.3 – Statistical analysis

SPSS software was used to conduct a three-way analysis of variance (ANOVA) to assess genotype (WT vs. ASM-/-) x time (baseline, 30 min. post-RTC, 60 min. post-RTC) x treatment (Ca^{2+} vs. EGTA) interaction of Fura-2 ratios at each stimulation frequency. The statistical significance was set at an α-level of 0.05. Fisher's least significant difference was used for all post-hoc analyses. Appendix contains the SPSS outputs for significant comparisons.

Chapter 3: Results

3.1 – Single muscle fiber responsiveness

A total of 6 mice were used from each group (WT vs. ASM-/-), and 64 single muscle fibers underwent the RTC protocol. Only fibers responding to all frequencies during baseline measurements were recorded. Table 1 shows the number of fibers responding to stimulus at baseline, 30 minutes post-RTC, and 60 minutes post-RTC. From the WT mice, 33 single muscle fibers were analyzed, and 16 of the 33 were treated with EGTA instead of Ca^{2+}. Of the WT fibers, 21 (64%) fibers responded to all stimulation frequencies 30 minutes after RTC. By 60 minutes post-RTC, only 16 (48%) WT fibers were responsive to all stimulation frequencies. At 60 minutes post-RTC, 8 of 17 (64%) and 8 of 16 (50%) WT fibers responded after RTC in the presence of Ca^{2+} or EGTA, respectively.

From the ASM-/- group, 31 single muscle fibers were analyzed, and 15 of the 31 ASM-/- fibers were treated with EGTA while 16 were treated with Ca^{2+}. Of the ASM-/- fibers, 21 (68%) fibers responded to all frequencies 30 minutes after RTC. By 60 minutes post-RTC, only 12 (39%) ASM-/- fibers were responsive to all stimulation frequencies. At 60 minutes post-RTC, 5 of 16 (31%) and 7 of 15 (46%) ASM-/- fibers responded after RTC in the presence of Ca^{2+} or EGTA, respectively. There were no significant differences in number of fibers responding between all groups at 30 or 60 minutes post-RTC.

The average exposure time to RTC for all groups can be seen in Table 1. Briefly, the average time fibers were exposed to RTC was 3.80 ± 0.18 minutes (mean ± standard error). Average time (minutes) to 50% initial peak Fura-2 ratio during RTC of WT $+Ca^{2+}$ (4.64 ± 0.27), WT +EGTA (4.47 ± 0.38), and ASM-/- $+Ca^{2+}$ (3.53 ± 0.26) were

significantly greater ($p<0.05$) than ASM-/- +EGTA (2.42 ± 0.14). Average time to 50% initial peak Fura-2 ratio during RTC of ASM-/- $+Ca^{2+}$ (3.53 ± 0.26) was significantly lower than WT $+Ca^{2+}$ (4.64 ± 0.27). There were no significant differences in average time to 50% initial peak Fura-2 ratio during RTC between WT +EGTA and ASM-/- $+Ca^{2+}$ or between WT groups.

Table 1. Number of fibers responding to stimuli and exposure time to RTC protocol

	Baseline	Time (minutes)	30 min. post-RTC	60 min. post-RTC
WT $+Ca^{2+}$	17	4.64 ± 0.27	11 (64%)	8 (47%)
WT +EGTA	16	4.47 ± 0.38	10 (62%)	8 (50%)
ASM-/- $+Ca^{2+}$	16	3.53 ± 0.26*	12 (75%)	5 (31%)
ASM-/- +EGTA	15	2.42 ± 0.14*#$	9 (60%)	7 (46%)

Data shown are mean ± SE. * $p<0.05$ vs. WT $+Ca^{2+}$, # $p<0.05$ vs. ASM-/- + Ca^{2+}, $ $p<0.05$ vs. WT +EGTA

3.2 – Ca^{2+} handling

There was no significant genotype (WT vs. ASM-/-) x treatment (Ca^{2+} vs. EGTA) x time (baseline, 30 min. post-RTC, 60 min. post-RTC) interaction for Fura-2 ratios at 0Hz, but there was a trend to significance at 10Hz ($p=0.057$), 30Hz ($p=0.059$), and 50Hz ($p=0.065$). Conversely, there was significant genotype x treatment x time interaction ($p<0.05$) for peak Fura-2 ratio at 70Hz, 100Hz, 120Hz, and 150Hz.

During baseline measurements of single muscle fibers treated with Ca^{2+}, ASM-/- fibers had significantly lower peak Fura-2 ratios ($p<0.05$) than WT fibers (see Figure 5B). Specifically, peak Fura-2 ratios of ASM-/- fibers treated with Ca^{2+} during baseline measurements were significantly lower compared to WT fibers treated with Ca^{2+} ($p<0.01$) at 70Hz (0.853 ± 0.050 vs. 1.046 ± 0.065), 100Hz (0.924 ± 0.063 vs.1.180 ± 0.080), 120Hz (0.948 ± 0.062 vs. 1.237 ± 0.077), and 150Hz (0.988 ± 0.067 vs. 1.233 ± 0.085).

In WT fibers during baseline measurements, treatment with EGTA elicited significantly lower peak Fura-2 ratios ($p<0.05$) compared to Ca^{2+} treatment (see Figure 5C). Specifically, peak Fura-2 ratios during baseline of WT fibers treated with EGTA were significantly lower than WT fibers treated with Ca^{2+} at 70Hz (0.947 ± 0.063 vs. 1.046 ± 0.065), 100Hz (1.028 ± 0.073 vs. 1.180 ± 0.080), 120Hz (1.050 ± 0.074 vs. 1.237 ± 0.077), and 150Hz (1.029 ± 0.073 vs. 1.233 ± 0.085). In ASM-/- fibers during baseline measurements, there were no significant differences in peak Fura-2 ratios between Ca^{2+} and EGTA treatment (see Figure 5D).

Peak Fura-2 ratio was significantly ($p<0.05$) lower in ASM-/- fibers treated with EGTA than WT fibers treated with Ca^{2+} at 120Hz (1.047 ± 0.079 vs. 1.233 ± 0.085) (see Figure 5A). However, the difference in peak Fura-2 ratios between WT fibers treated with Ca^{2+} and ASM-/- fibers treated with EGTA trended towards significance at 50Hz ($p=0.063$), 100Hz ($p=0.059$), and 150Hz ($p=0.061$).

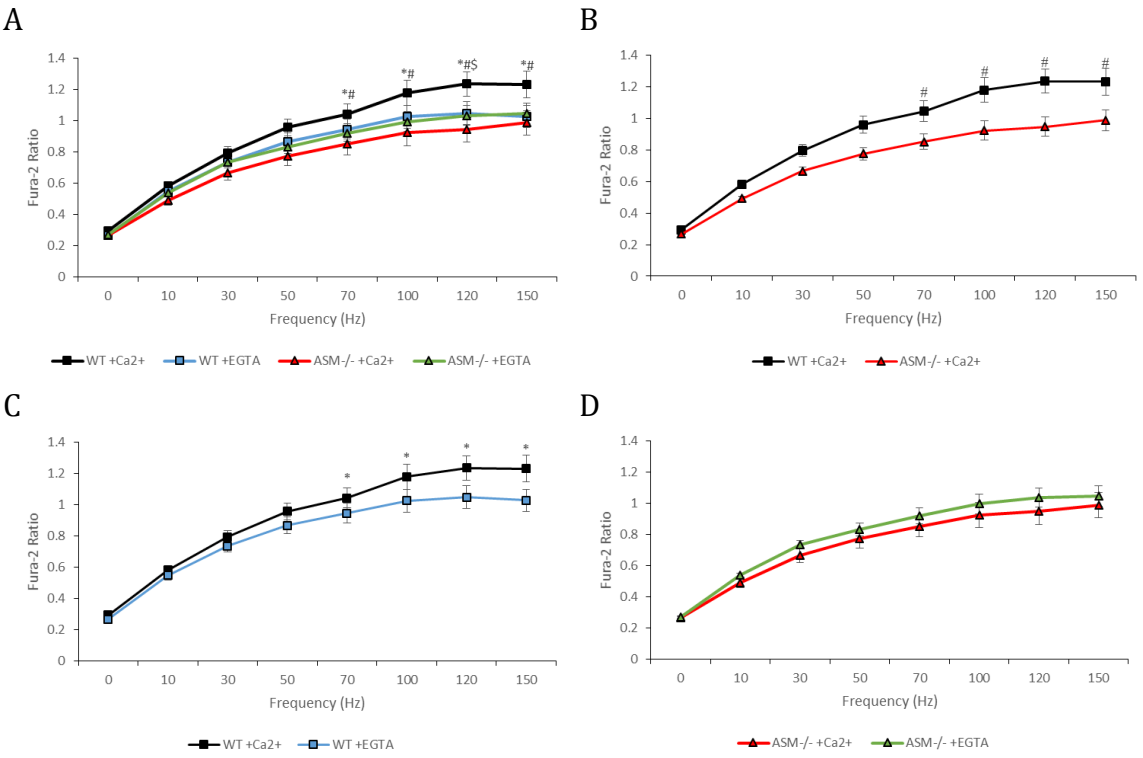

Figure 5. Baseline peak Fura-2 ratios. A) Peak Fura-2 ratios of WT treated with Ca^{2+} (n=17), WT treated with EGTA (n=16), ASM-/- treated with Ca^{2+} (n=16), ASM-/- treated with EGTA (n=15). B) Peak Fura-2 ratios between WT and ASM-/- treated with Ca^{2+}. C) Peak Fura-2 ratios in WT between Ca^{2+} and EGTA treatment. D) Peak Fura-2 ratios in ASM-/- between Ca^{2+} and EGTA treatment. Data shown are mean ± SE. * $p<0.05$ for WT +Ca^{2+} vs. WT +EGTA, # $p<0.05$ for WT +Ca^{2+} vs. ASM-/- +Ca^{2+}, $ $p<0.05$ for WT +Ca^{2+} vs. ASM-/- +EGTA.

In WT fibers treated with Ca^{2+}, there were no significant differences between baseline, 30-minutes post-RTC, and 60 minutes post-RTC in peak Fura-2 ratios at all frequencies (see Figure 6A). However, in WT fibers treated with EGTA, both 30 minutes post- and 60 minutes post-RTC measurements had significantly higher peak Fura-2 ratios ($p<0.05$) than baseline measurements at 70Hz or higher frequencies (see Figure 6C). Specifically, peak Fura-2 ratios of WT fibers treated with EGTA were significantly higher at 30 minutes post-RTC compared to baseline ($p<0.05$) at 70Hz (1.039 ± 0.049 vs. 0.947 ±

0.063) and 150Hz (1.168 ± 0.056 vs. 1.029 ± 0.073). Similarly, peak Fura-2 ratios of WT fibers treated with EGTA were significantly higher at 60 minutes post-RTC compared to baseline ($p<0.05$) at 70Hz (1.062 ± 0.050 vs. 0.947 ± 0.063), 100Hz (1.171 ± 0.061 vs. 1.028 ± 0.073), and 150Hz (1.209 ± 0.065 vs. 1.029 ± 0.073).

In ASM fibers treated with Ca^{2+}, both 30 minutes post- and 60 minutes post-RTC measurements had significantly higher peak Fura-2 ratios ($p<0.05$) than baseline measurements at 70Hz or higher (see Figure 6B). Peak Fura-2 ratios of ASM-/- fibers treated with Ca^{2+} were significantly higher at 30 minutes post-RTC compared to baseline ($p<0.05$) at 120Hz (1.061 ± 0.089 vs. 0.948 ± 0.062) and 150Hz (1.050 ± 0.088 vs. 0.988 ± 0.067). Similarly, peak Fura-2 ratios of ASM-/- fibers treated with Ca^{2+} were significantly greater ($p<0.05$) at 60 minutes post-RTC than baseline at 70Hz (1.021 ± 0.085 vs. 0.853 ± 0.050), 100Hz (1.108 ± 0.119 vs. 0.924 ± 0.063), 120Hz (1.182 ± 0.133 vs. 0.948 ± 0.062), and 150Hz (1.168 ± 0.161 vs. 0.988 ± 0.067). There were no significant differences in peak Fura-2 ratios between ASM-/- and WT fibers treated with Ca^{2+} during 30 minutes and 60 minutes post-RTC.

In ASM-/- fibers treated with EGTA, neither the 30 minutes post- nor 60 minutes post-RTC measurements were significantly different in peak Fura-2 ratios ($p<0.05$) from baseline measurements. However, peak Fura-2 ratios 30 minutes post-RTC (1.022 ± 0.091) was significantly greater ($p<0.05$) than 60 minutes-post RTC (0.897 ± 0.088) at 70Hz (see Figure 6D).

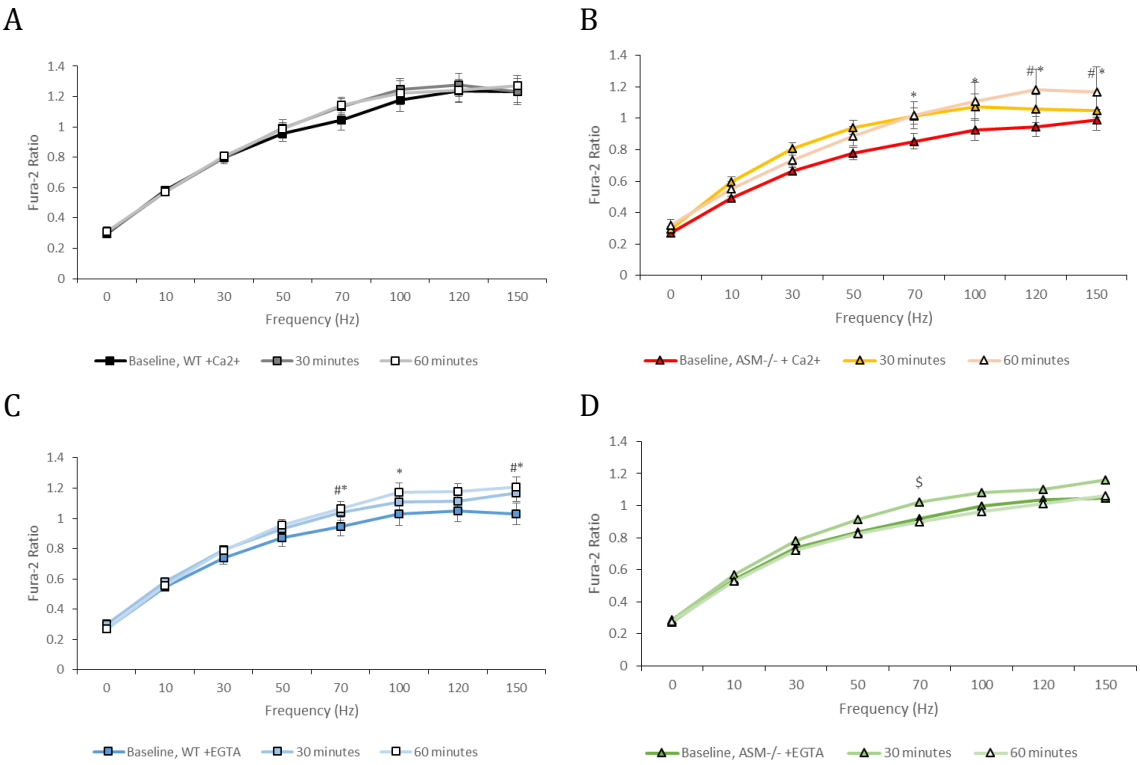

Figure 6. Comparisons of peak Fura-2 ratios between baseline, 30 minutes post-RTC, and 60 minutes post-RTC. A) Peak Fura-2 ratios of WT fibers treated with Ca^{2+} during all three time measurements (baseline, n=17; 30 min post-RTC, n=11; 60 min post-RTC, n=8). B) Peak Fura-2 ratios of ASM-/- fibers treated with Ca^{2+} during all three time measurements (n=16; n=10; n=8). C) Peak Fura-2 ratios of WT fibers treated with EGTA during all three time measurements (n=16; n=12; n=5). D) Peak Fura-2 ratios of ASM-/- treated with EGTA during all three time measurements (n=15; n=9; n=7). Data shown are mean ± SE. # $p<0.05$ for baseline vs. 30 minutes post, * $p<0.05$ for baseline vs. 60 minutes post, $ $p<0.05$ for 30 minutes post vs. 60 minutes post.

Chapter 4: Discussion

4.1 – Interpretation of findings

Our findings demonstrate the ASM-/- fibers may have impairments in E-C coupling. Specifically, ASM-/- fibers exhibited lower peak Fura-2 ratios than WT fibers treated with Ca^{2+} during baseline measurements (Figure 5B). This suggests an impairment prior to or during SR-Ca^{2+} release. Propagation of the action potential across the sarcolemma and the T-tubules is important for SR-Ca^{2+} release (Lamb, 2009). Impairment of membrane depolarization greatly increases the extent of voltage-sensor dysfunction leading to a reduction of SR-Ca^{2+} release (Lamb, 2009). Damaged membranes in ASM-/- fibers remain unrepaired (Corrotte et al., 2013), and may have a reduced capacity to propagate an action potential leading to diminished SR-Ca^{2+} release. Peak Fura-2 ratios during baseline measurements in WT treated with EGTA were similar to responses in ASM-/- fibers treated with Ca^{2+} or with EGTA. This might be explained by two mechanisms, which are not exclusive to each other. First, lack of extracellular Ca^{2+} through the use of EGTA inhibits lysosomal exocytosis and membrane repair (Reddy et al., 2001), leaving the plasma membrane injured, thereby reducing its capacity to transmit an action potential, and subsequently lowering SR-Ca^{2+} release. Second, extracellular Ca^{2+} removal has been reported to elicit a decline in resting membrane potential and tension production (Curtis, 1963; Jenden & Reger, 1963). The reduced membrane potential diminishes depolarization effectiveness and Ca^{2+} release, thus resulting in force production decline (Curtis, 1963). Therefore, impairments in E-C coupling can be elicited through ASM deficiency and reduced extracellular Ca^{2+} in muscle fibers.

The present results show that E-C coupling failure following repeated contractions is greater in ASM-/- fibers compared to WT fibers. Specifically, only 39% of measured ASM-/- fibers responded to all stimulation frequencies during the 60 minutes post-RTC measurements compared to 48% of WT fibers (see Table 1). Furthermore, both ASM-/- groups reached 50% of their initial peak Fura-2 ratio during the RTC protocol faster than the WT fibers treated with Ca^{2+} (see Table 1) suggesting an inability to repeatedly regenerate a membrane potential and activate optimum Ca^{2+} release.

Peak Fura-2 ratios of WT fibers treated with Ca^{2+} returned to baseline measurement levels post-RTC. No difference in peak Fura-2 ratio in WT fibers treated with Ca^{2+} after RTC was unexpected. Maximum tension (Allen, Lee, & Westerblad, 1989; Westerblad & Allen, 1991) has been shown to recover fully after a bout of fatigue in mouse single muscle fibers, although Fura-2 ratio has a prolonged reduction after fatigue, explaining the long-term suppression of force at low stimulation frequencies (Westerblad et al. 1993; Chin et al. 1997). Thus, we expected a reduction in Fura-2 ratio after RTC. However, in this study using collagenase-digested single muscle fiber preparations, a reduction in peak Fura-2 ratio after RTC was not observed. This is consistent with a prior study from our lab (Mázala et al., 2015), and appears to be a difference between repeated isotonic and isometric contractions.

It was initially predicted that both ASM-/- fibers treated with Ca^{2+} and WT fibers treated with EGTA would exhibit reduced recovery capacity after RTC. However, both ASM-/- fibers treated with Ca^{2+} (Figure 6B) and WT fibers treated with EGTA (Figure 6C) had elevated peak Fura-2 ratios during both post-RTC measurements compared to their respective baseline measurement levels. A compromised membrane may allow the influx

of extracellular Ca^{2+} during RTC in ASM-/- fibers, which is then taken up by the SR, increasing its capacity for SR-Ca^{2+} release during subsequent activations. This may be a potential mechanism to explain the recovery behavior in ASM-/- fibers after repeated contractions. Ca^{2+}-induced Ca^{2+} release, whereby an increase in intracellular Ca^{2+} induces the release of Ca^{2+} from the SR (Endo, 2009), might also explain our post-RTC measurement findings. An injured membrane in ASM-/- fibers could similarly allow the influx of Ca^{2+} during RTC, thus eliciting Ca^{2+}-induced Ca^{2+} release during post-RTC measurements. Influx of Ca^{2+} is likely minimal for WT fibers treated with EGTA, but it may be possible for Ca^{2+} to accumulate in the T-tubules during RTC (Bianchi & Narayan, 1982), via Ca^{2+}-ATPase pumps found in the T-tubule membrane (Sacchetto et al., 1996). Ca^{2+} accumulation in the T-tubule might be sufficient to recover the reduced membrane potential elicited by Ca^{2+} deprivation, resulting in improved propagation of an action potential and greater SR-Ca^{2+} release. Thus, while these findings were unexpected, they demonstrate the requirement for both ASM and extracellular Ca^{2+} in the baseline E-C coupling. Further, ASM and extracellular Ca^{2+} are required for the enhanced E-C coupling post-RTC as fibers from ASM-/- mice with zero extracellular Ca^{2+} did not have an enhanced Fura-2 ratio following repeated tetanic contractions. It should be noted that, to our knowledge, there is no prior research that explores recovery from repeated tetanic contractions in ASM-/- fibers and WT fibers in the absence of extracellular Ca^{2+}.

4.2 – Potential limitations and future directions

Although we suggest that inhibited membrane repair may be associated with E-C uncoupling in ASM-/- and WT fibers, the uncertainty of membrane damage in these fibers

makes it difficult to fully establish this relationship. There is some evidence to suggest that membranes of ASM-/- fibers are injured (Andrews, personal communication); however, it is uncertain if the single muscle fibers that we have evaluated in the current study had compromised membranes. We were unable to ascertain if inhibited membrane repair through ASM deficiency or Ca^{2+} deprivation is the primary contributor to E-C uncoupling in ASM-/- and WT muscle fibers. It is unknown if membrane wounding occurred in these fibers during the isolation procedure or the stimulation protocol. This uncertainty could be answered in a future study using propidium iodide, a membrane impermeable dye (Butler et al., 2002; Idone et al., 2008), which only enters muscle fibers upon injury. Specifically, propidium iodide could be utilized during the stimulation protocol to demonstrate if single or repeated tetanic contractions elicit membrane wounding in ASM-/- fibers. Other future studies replicating our results using techniques such as glass bead injury, SLO (Corrotte et al., 2013), or laser ablation (Jimenez et al., 2015), to wound the membranes with improved certainty would more directly test the hypothesis that impaired membrane repair is responsible for E-C uncoupling. Another potential mechanism for membrane injury during contraction could be related to membrane instability caused by over accumulation of sphingomyelin (Gabandé-Rodriguez, 2014). Thus, given these additional factors, it is critical to demonstrate membrane injury in ASM-/- fibers to better establish the relationship between impaired membrane repair and E-C uncoupling.

The ASM-/- fibers in our study demonstrate E-C coupling disruption. While these data support a potential relationship between impaired membrane repair and E-C uncoupling, there are other possibilities that might contribute to the observed E-C coupling disruption. Other possible causes for the impairments in E-C coupling could include

DHPR activation failure, a communication impairment between DHPR and the RyR, and a diminished SR-Ca^{2+} uptake rate (Lamb, 2009). In order to rule out these possibilities, a future study should assess the content and sensitivity of DHPR and RyR in ASM-/- fibers. Decreased content or sensitivity of DHPR and RyR could potentially diminish SR-Ca^{2+} release (Lamb, 2009). Other possibilities for E-C uncoupling should therefore be explored before concluding that membrane repair impairment is the primary contributor to E-C coupling disruption in ASM-/- muscle.

Although protease activity was not investigated in this study, proteases may also play a role in prolonged E-C coupling impairment in ASM-/- muscle and should be investigated in future studies as well. Specifically, it has been proposed that Ca^{2+}-activated proteases such as calpains could play a role in the prolonged disruption of E-C coupling in some muscle diseases (Lamb et al., 1994; Verburg et al., 2005), and thereby implicating a possible role in NPD. Several studies have demonstrated that the activation of calpains (calpain-3 and μ-calpain) by $[Ca^{2+}]_i$ occurs within the physiological range of muscle contractions (0.5 – 3.0μM) (Branca, Gugliucci, Bano, Brini, & Carafoli, 1999; Murphy et al., 2007; Murphy & Lamb, 2009). The specific downstream targets of calpains are still unclear, but there is evidence to suggest that they participate in the process of cytoskeleton remodeling and interact closely with the plasma membrane (Gailly, De Becker, Van Schoor, & Gillis, 2007). Excessive muscle stimulation or pharmacologically-induced increase in intracellular Ca^{2+} levels has been shown to simultaneously activate calpains and the proteolysis of junctophilin, the latter of which is a key protein in mediating the SR and T-tubule interaction at the triad (Murphy et al., 2013), and facilitating the assembly of the DHPR with other proteins involved in E-C coupling (Golini et al., 2011). Other possible

calpain substrates include, but are not limited to, RyR, sarcoplasmic/endoplasmic reticulum calcium ATPase (SERCA), dystrophin, desmin, titin, tropomyosin, and troponin (Croall & Ersfeld, 2007; Goll, Thompson, Li, Wei, & Cong, 2003), all of which play important roles in plasma membrane integrity and E-C coupling.

Cathepsin B is yet another type of protease with a potential role in the prolonged disruption of E-C coupling in ASM-/- muscle fibers. According to Moles and colleagues (2012), there was increased expression and increased activation of cathepsin B in ASM-/- mice. Similarly, Gabandé-Rodriguez and colleagues (2012) also noted increased activity of cathepsin B in ASM-/- fibroblasts. The accumulation of sphingomyelin due to the lack of ASM has been shown to compromise the integrity of lysosomes as well (Gabandé-Rodriguez et al., 2014), thereby resulting in the release of cathepsin B from the lysosome into the cytosol. Cathepsin B has been further implicated in plasma membrane repair (Castro-Gomes et al., 2015), signaling pathways of apoptosis (Moles et al., 2011), and intracellular protein degradation (Gabandé-Rodriguez et al., 2014). As such, future studies should investigate the potential role of calpains and cathepsin B in the prolonged disruption of E-C coupling and muscle weakness observed in ASM deficiency and NPD.

Finally, research on ASM deficiency has largely focused on neuropathology. Therefore, the timeline of disease progression has been primarily tied to the events of neural degeneration. For example, in the study conducted by Macauley and colleagues (2008), ASM-/- mice begin to exhibit performance deterioration and degeneration of cerebellar Purkinje cells after 7 weeks of age. However, disease progression has not been well documented in skeletal muscle. Consequently, it is possible that muscular degeneration or dysfunction occurs earlier than the first appearance of neural deterioration.

Consistently, Marcuzzo and colleagues (2011) reported muscle atrophy at 8 weeks of age in the G93A-SOD1 mouse model for ALS, while MRI evidence of neurodegeneration was only apparent at 10 weeks of age. Due to the general dearth of research exploring skeletal muscle pathology in ASM-/- mice, the relative severity of skeletal muscle dysfunction at 8 weeks of age is unknown. As such, a better understanding of the disease progression in skeletal muscle may better explain how E-C uncoupling begins in ASM deficiency and NPD.

4.3 – Conclusion

This study is the first to evaluate intracellular Ca^{2+} handling and impairment in E-C coupling due to repeated contractions in muscle fibers lacking ASM. While NPD has been primarily treated as a neurological and visceral disorder, the cause of muscle weakness may, at least in part, have an origin in the muscle itself. Evidence from this study lends support to the notion that muscles deficient in ASM have some E-C coupling impairment and reduced fatigue resistance. Furthermore, Ca^{2+} deprivation in skeletal fibers elicited similar E-C uncoupling responses as fibers deficient in ASM. Therefore, our results demonstrate that impaired membrane repair due to ASM deficiency may contribute to E-C coupling disruption in ASM -/- mice.

Chapter 5: Review of Literature

5.1 – Skeletal muscle plasticity

Skeletal muscle has a high degree of plasticity and is responsive to various stimuli, for example, exercise training, aging, disuse, and various diseases can cause changes in skeletal muscle (Holloszy, 1967; Marimuthu, Murton, & Greenhaff, 2011). Skeletal muscle adaptations can be unique to each person, especially when pertaining to exercise training, as has been shown in previous studies (Hubal et al., 2005; Simoneau & Bouchard, 1995). There have been multiple studies investigating the mechanisms behind adaptations in healthy muscle, as well as those examining molecular and cellular changes in diseased muscle (Allen et al., 2005; Bonaldo & Sandri, 2013; Chargé & Rudnicki, 2004; Chin et al. 2014; Mázala et al., 2015; Whitehead et al., 2006). However, the mechanisms behind these diseased states are far less understood than healthy muscles. As such, it is imperative to understand the mechanisms underlying the pathology of the disease in order to develop better interventions used to reduce disease severity and improve functionality.

5.2 – Sphingomyelinase and its downstream products

The gene coding for acid sphingomyelinase (ASM), *SMPD1*, for humans is located on chromosome 11p15.1-11p15.4, spans about 6 kilobases, and consists of six exons and five introns (Jenkins et al., 2009). Three variants can manifest from a single mRNA, but only the type 1 transcript will result in a functional ASM enzyme (Jenkins et al., 2009). The full-length cDNA of the type 1 transcript has an open-reading frame of 1890bp and will give rise to a polypeptide comprised of 629 amino acids (Jenkins et al., 2009). Murine ASM is about 82% similar to human ASM and is located on chromosome 7 (Jenkins et al.,

2009). *SMPD1* can be subjected to epigenetic regulation via methylation, and genetic imprinting at the *SMPD1* locus may contribute to the heterogeneity of patients with NPD/B (Jenkins et al., 2009). ASM plays a critical role in the pathophysiology of NPD/A and NPD/B.

Sphingomyelinases are enzymes that hydrolyze sphingomyelin, a type of sphingolipid abundantly found in plasma membranes (Smith & Schuchman, 2008), into ceramide and phosphorylcholine. There are six classifications of sphingomyelinases according to Goñi and Alonso (2002). Specifically, these classifications are acid, secretory, neutral magnesium (Mg^{2+})-dependent, neutral Mg^{2+}-independent, alkaline, and bacterial sphingomyelinase (Goñi & Alonso, 2002). The two most investigated enzyme types are ASM and secretory sphingomyelinase (SSM). Both ASM and SSM arise from the *SMPD1* gene (Goñi & Alonso, 2002; Smith & Schuchman, 2008). The common protein precursor to both ASM and SSM is trafficked to either lysosomes (ASM) or to the Golgi secretory pathway (SSM) (Goñi & Alonso, 2002). Zinc (Zn^{2+}) may play an important role for both ASM and SSM (Goñi & Alonso, 2002; Jenkins et al., 2009). In ASM, Zn^{2+} is acquired during the transport to the lysosome (Goñi & Alonso, 2002; Jenkins et al., 2009). The secretory type can be activated by various concentrations of Zn^{2+}, but Zn^{2+}-independent forms may exist (Goñi & Alonso, 2002). Furthermore, the activity of ASM can be enhanced with phosphatidylinositol or inhibited by the phosphorylated forms of phosphatidylinositol (Jenkins et al., 2009). As the role of ASM in human physiology has largely been performed in loss-of-function studies, the specific differences between the metabolic and biological roles of ASM have yet to be determined (Jenkins et al., 2009).

The primary target and product of ASM play important roles in the plasma membrane and cell signaling. Sphingomyelin is a major lipid component in all mammalian membranes and is comprised of a phosphorylcholine bound to a ceramide (Smith & Schuchman, 2008). Sphingomyelin is the most prevalent sphingolipid, and is located in the outer leaflet of the membrane (Smith & Schuchman, 2008). When sphingomyelin is hydrolyzed by ASM into ceramide, the resulting product can change the physical properties of the membrane, have direct ceramide-protein interactions, or facilitate other protein-protein interactions (Smith & Schuchman, 2008). Ceramide can also be metabolized by ceramidases into sphingosine, which can further be phosphorylated into sphingosine-1-phosphate (Smith & Schuchman, 2008). Sphingosine is a molecule associated with growth arrest and sphingosine-1-phophate promotes cell survival; therefore, the relative amounts of these two molecules may determine the effect of ASM and cell fate (Smith & Schuchman, 2008).

5.3 – Background on Niemann-Pick disease

Niemann-Pick disease (NPD) can affect a wide variety of body systems, and the disease symptoms can range in severity. This disease has four main types: type A, type B, type C1, and type C2. Patients with type A or type B have some mutation of the *SMPD1* gene resulting in an inherited deficiency of ASM (Irun et al., 2013). According to Irun and colleagues (2013), there are at least 15 different mutations of the *SMPD1* gene. The shortage of ASM reduces the breakdown of the lipid sphingomyelin, causing its accumulation in cells (Gabandé-Rodriguez et al., 2014). Over accumulation may cause the cells to malfunction or die (Gabandé-Rodriguez et al., 2014). This disorder occurs in ~1

in every 250,000 births, with a higher prevalence in eastern and central Europeans, specifically, those of Ashkenazi Jewish descent (Meikle, Hopwood, Clague, & Carey, 1999). In particular, this disease affects ~1 in 40,000 individuals within the Ashkenazi population (Meikle et al., 1999). Patients with NPD type A (NPD/A) are typically infants and exhibit an eye-abnormality called a cherry-red sport (Gumbinas, Larsen, & Liu, 1975; McGovern, Aron, Desnick, & Wasserstein, 2006). They also tend to develop hepatosplenomegaly (i.e. enlarged liver and spleen), around 3 months of age and fail to gain weight and thrive (McGovern et al., 2006). The mental development of infants with NPD/A progresses normally up until the age of 1 year, at which point they begin to show progressive psychomotor regression and loss of mental abilities (McGovern et al., 2006). Children with NPD/A are further likely to develop interstitial lung disease that can lead to frequent lung infections and respiratory failure (Gumbinas et al., 1975; McGovern et al., 2006). Patients with NPD/A rarely survive past early childhood (Gumbinas et al., 1975; McGovern et al., 2006).

Patients with NPD type B (NPD/B) have similar, albeit milder symptoms, compared to patients with NPD/A. In patients with NPD/B, relevant signs and symptoms generally develop during mid-childhood to teenage years (McGovern et al., 2013). As with infant patients with NPD/A, patients with NPD/B often develop hepatosplenomegaly, lung infections, and thrombocytopenia (i.e. low platelet count) (McGovern et al., 2013; Wasserstein et al., 2004). However, their bone mineralization is slowed, thus resulting in short stature. Unlike patients with NPD/A, only one-third of individuals with NPD/B have the cherry-red spot eye or other neurological impairment (Wasserstein et al., 2004). Most individuals with NPD/B survive into adulthood (Wasserstein et al., 2004).

Patients with Niemann-Pick type C1 and C2 (NPD/C) have somewhat similar symptoms to NPD/A and NPD/B, but differ in their genetic cause. Mutations in either *NPC1* or *NPC2* dictate the development of NPD/C (Garver et al., 2007; Sturley, Patterson, Balch, & Liscum, 2004). These genes encode for proteins that are involved in the transportation of lipids (Garver et al., 2007; Sturley et al., 2004), within all cell types (Fagerberg et al., 2014). These mutations result in a deficit in functional proteins resulting in an accumulation of lipids within the cells (Garver et al., 2007; Sturley et al., 2004). This lack of lipids in their proper locations leads to additional impairments of certain cell functions, e.g., cell membrane formation (Garver et al., 2007; Sturley et al., 2004). Both the over accumulation of lipids and cell dysfunction results in eventual cell death and organ damage (Garver et al., 2007; Sturley et al., 2004). NPD/C is estimated to affect 1 in 150,000 individuals, with a higher prevalence in people of French-Acadian descent in Nova Scotia (Meikle et al., 1999). Symptoms of type C include ataxia (coordination difficulty), vertical supranuclear gaze palsy (inability to moves eyes vertically), dystonia (poor muscle tone), severe liver disease, and interstitial lung disease (Garver et al., 2007). Affected individuals have difficulty speaking and swallowing, which worsens over time and eventually interferes with feeding. Intellectual function in individuals with NPD/C also decline with age (Garver et al., 2007). These symptoms begin to appear in childhood, and some with NPD/C survive into adulthood.

5.4 – Mouse model for NPD

In 1995, Horinouchi and colleagues created the first mouse model of NPD through gene targeting and embryo transfer techniques. The investigators constructed an *ASM*

replacement vector that was inserted into the *ASM* gene (*SMPD1*) of mice to disrupt the coding sequence (Horinouchi et al., 1995). The diseased animals exhibited severe neurodegenerative progression and died by 8 months of age. These animals appeared normal at birth, but developed symptoms such as ataxia and tremors around 8 weeks of age. By 12 to 16 weeks, the mice studied by Horinouchi and colleagues (1995) exhibited difficulty feeding and became lethargic and unresponsive to stimuli. By 4 months, all mice exhibited severe ataxia. Death in all mice occurred between 6 to 8 months. Notably, at the time of death, all the diseased mice displayed an observably 'hunched' appearance. Horinouchi and colleagues (1995) found no ASM activity in the liver, lung, spleen, kidney, heart, and brain of the ASM knockout (ASM-/-) mice, and 50% activity in the same tissues of the heterozygous mice.

A separate study conducted by Macauley and colleagues (2008) added to the results of the previous study completed by Horinouchi and colleagues (1995) by investigating the time course of neurodegeneration and lysosomal pathology in the nervous system of ASM-/- mice. Macauley and colleagues (2008) utilized rotarod tests and silver degeneration staining to assess behavioral and neurobiological degeneration, respectively (Macauley et al., 2008). Rotarod testing employs a rotating rod to force motor activity on the mice, and results from this test help to evaluate balance, grip strength, and motor coordination (Jones & Roberts, 1968). Silver degeneration staining exploits the increased affinity of silver to impregnate wounded nerves as an assessment for neural degeneration (Switzer III, 2000). Supporting the findings of Horinouchi et al. (1995), ASM-/- mice performed just as well as the control mice on the rotating rod tests at 5 to 7 weeks of age; however, their performance severely declined between 7 and 20 weeks of age (Macauley et al., 2008).

Similarly, degeneration of Purkinje cells of the cerebellum began by 7 weeks of age with complete deterioration by 20 weeks (Macauley et al., 2008).

There is some evidence to indicate that the plasma membranes of ASM-/- mice display membrane instability due to over accumulation of sphingomyelin (Butler et al., 2002; Gabandé-Rodriguez et al., 2014). For example, Butler and colleagues (2002) investigated the cellular structures of spermatozoa from ASM-/- mice to better understand the reproductive pathogenesis in NPD. In particular, Butler and colleagues (2002) found that 86.6% of their spermatozoa had membrane wounding with propidium iodide (PI) staining, a probe for membrane injury (Butler et al., 2002). Comparatively, only 40.8% of spermatozoa from wild-type mice had evidence of membrane damage (Butler et al., 2002). Furthermore, mature spermatozoa from ASM-/- mice had elevated levels of sphingomyelin and cholesterol. Morphological abnormalities, such as bends and kinks in the tail of the spermatozoa, were completely resolved after incubation in a dilute detergent, thereby demonstrating that these morphological abnormalities were a direct consequence of lipid accumulation (Butler et al., 2002). In a separate study by Gabandé-Rodriguez and colleagues (2014), neurons of ASM-/- mice show a buildup of sphingomyelin and an increased cytosolic release of cathepsin B compared to wild-type mice. Additionally, wild-type mice treated with sphingomyelin demonstrated similar elevated cytosolic release, further supporting the role of sphingomyelin accumulation in membrane instability (Gabandé-Rodriguez et al., 2014).

5.5 – Mechanisms of plasma membrane repair

The plasma membrane, also known as the sarcolemma in muscle, is an important component in the excitation-contraction coupling pathway (E-C coupling). It carries the electrical signal generated at the neuromuscular junction to the transverse tubules which activates dihydropyridine receptors, eventually leading to calcium release from the sarcoplasmic reticulum (SR) and cross bridge formation. A damaged plasma membrane may directly or indirectly disrupt E-C coupling. Yeung and colleagues (2002) suggested that T-tubule rupture from eccentric contractions could decrease inward action potential, increase Ca^{2+} influx, and increase sodium (Na^{+}) influx. Both decreased action potential and increased Ca^{2+} influx can lead to decreased SR-Ca^{2+} release (Yeung et al., 2002). An increase in Na^{+} influx raises the osmotic load of the T-tubule system and results in localized swelling (Yeung et al., 2002). The T-tubule is a specialized continuation of the sarcolemma, and thus these findings are expected to reflect changes to the sarcolemma as well. It is also known that impaired plasma membrane repair may accelerate disease pathology in some forms of muscular dystrophy (Bansal & Campbell, 2004). Therefore, it is imperative that there be a system capable of repairing the plasma membrane in order to maintain the integrity of E-C coupling and muscle activation.

Miyake and McNeil (1995) suggested that wounds to the plasma membrane are repaired via a patch mechanism. In their study, bovine retinal microvascular endothelial (BRME) and NIH 3T3 cells were wounded through scratch loading, a method that runs the tip of a syringe through cell monolayers to induce mechanical stress (Miyake & McNeil, 1995). Transmission electron microscopy showed that vesicles accumulated within the cytoplasm of these cells around the damage site (Miyake & McNeil, 1995). Miyake and McNeil (1995) also employed FM1-43, a membrane specific dye, to demonstrate that

wounding in these cells triggered a Ca^{2+}-dependent exocytosis from one or more internal membrane compartments near the injury site (Miyake & McNeil, 1995). The investigators further showed that the size of the cell increased after injury (Miyake & McNeil, 1995). In general, Miyake and McNeil's findings (1995) suggested that some internal membrane compartment near the injury site fused with the plasma membrane, resulting in a larger and repaired cell.

Togo and colleagues (2000) suggested that reduced membrane tension was necessary for cell membrane repair. Laser tweezers were also used to tether the membrane of Swiss 3T3 fibroblasts, and membrane tension was measured after membrane injury during repair (Togo et al., 2000). Togo and colleagues (2000) found that in a normal Ca^{2+} Ringer's solution (1.8mM Ca^{2+}), membrane tension decreased dramatically to approximately 60% of initial tension after injury, and gradually recovered to initial values at an average of 78.3s. Although the rate of tension decline was double after second injury in the same, normal Ca^{2+} Ringer's solution, tension decline was not observed in low Ca^{2+} Ringer's solution (0.1mM Ca^{2+}) (Togo et al., 2000). The investigators thus suggested that a new vesicle pool was required to properly seal a second wound (Togo et al., 2000). Generation of new vesicles involves protein kinase C (PKC)-dependent and brefeldin A (BFA)-sensitive pathways, and inhibitors of these pathways were used to slow or inhibit tension decline in the second injury (Togo et al., 2000). Togo and colleagues (2000) believed that tension reduction was critical to membrane repair, so they attempted to facilitate recovery in the cells located in low Ca^{2+} Ringer's solution. In particular, the investigators artificially decreased membrane tension using cytochalasin D and found results of recovery similar to recovery in cells in normal Ca^{2+} Ringer's solution (Togo et

al., 2000). With these results, Togo and colleagues (2000) subsequently suggested that membrane tension is an important component during membrane repair.

A year later, Reddy, Caler, and Andrews (2001) investigated the relationship between plasma membrane repair and Ca^{2+}-regulated exocytosis of lysosomes. They found the presence of Lamp-1, a glycoprotein normally on lysosomal membranes, on the plasma membrane of normal rat kidney epithelial (NRK) cells after scratch wounding (Reddy et al., 2001). Elevation of intracellular calcium concentration ($[Ca^{2+}]_i$) caused lysosomes to fuse with the plasma membrane (Reddy et al., 2001). Similar results were found in 3T3 mouse fibroblasts, L6E9 rat myoblasts, and Chinese hamster ovary cells (Reddy et al., 2001). In scratch assays, Lamp-1 staining was concentrated around the plasma membrane nearest to the injury site (Reddy et al., 2001). In order to determine the importance of extracellular Ca^{2+} after wounding, scratch assays were performed in solutions containing Ca^{2+} or 10mM EGTA (Reddy et al., 2001). The scratch tests performed in the presence of Ca^{2+} demonstrated the presence of Lamp-1 in 83% of injured NRK cells (Reddy et al., 2001). Conversely, only 22% of wounded NRK cells in EGTA exhibited Lamp-1 on their membrane surface (Reddy et al., 2001). Reddy and colleagues (2001) also examined the ubiquitously expressed synaptotagmin (Syt) VII and its potential role in the regulation of Ca^{2+}-dependent exocytosis. Scratch assays and staining indicated that the lumenal domain of Syt VII was exposed on the cell surface of wounded NRK cells, but not in injury-free cells (Reddy et al., 2001). Lysosomal exocytosis and membrane repair were both inhibited by recombinant Syt VII C_2A domain, anti-Syt VII C_2A antibodies, or cytosolic Lamp-1 domain antibodies. Reddy et al. (2001) further made use of the fibroblast-collagen-matrix contraction model to verify if the mechanism of membrane resealing in the NRK cells was

the same as the repair of cutaneous lesions. In this model, fibroblasts are embedded in a substrate-anchored collagen matrix and kept under mechanical tension (Reddy et al., 2001). When the tension is released, a contraction event of the collagen matrix occurs and causes plasma membrane disruptions. These lesions were quickly sealed in a Ca^{2+}-dependent fashion (Reddy et al., 2001). Additionally, lactate dehydrogenase (LDH), a marker for membrane disruption, and β-hexosaminidase, a marker for lysosomal exocytosis, were detected in the supernatant shortly after tension release (Reddy et al., 2001). Reddy and colleagues (2001) ultimately concluded that lysosomes were Ca^{2+}-regulated and responsible for plasma membrane repair.

Another study by McNeil, Miyake, and Vogel (2003) investigated the importance of endomembranes in plasma membrane repair by comparing the resealing capabilities of red blood cells (RBCs), which lack endomembranes, with sea urchin eggs, fibroblasts, and neurons, all of which are rich in endomembrane compartments. These cells were wounded with a Ti:sapphire laser, and FM1-43 was used as the fluorescent membrane probe to assess membrane resealing (McNeil et al., 2003). Although the RBCs were unable to reseal rapidly after injury, wounds inflicted on sea urchin eggs, fibroblasts, and neurons, demonstrated fast and Ca^{2+}-dependent resealing (McNeil et al., 2003). McNeil, Miyake, and Vogel (2003) thus concluded that Ca^{2+} alone is not enough to elicit repair, and that endomembranes are required for rapid resealing.

While the exocytosis of some membranous compartment(s) is necessary for membrane repair, findings from Idone and colleagues (2008) suggest that a Ca^{2+}-dependent endocytosis is involved as well. Specifically, Idone and colleagues (2008) used the bacterial toxin streptolysin O (SLO) to create transmembrane pores in NRK cells. When

exposed to SLO in the presence of Ca^{2+}, NRK cells removed PI, a membrane impermeable dye, from inside the cell after 4 minutes (Idone et al., 2008). Conversely, NRK cells exposed to SLO without Ca^{2+} were unable to reseal until Ca^{2+} was added (Idone et al., 2008). Higher concentrations of SLO were correlated with less efficient resealing (Idone et al., 2008). Similar results were found in HEK-293 and HeLa cells treated with SLO as resealing was inhibited after adenosine triphosphate (ATP) depletion (Idone et al., 2008). The researchers also performed time-lapse video microscopy using Fluo-3, which measures intracellular Ca^{2+}, to determine the kinetics of SLO pore repair. SLO pore repair occurred quickly in less than 30 seconds, and the rapidness of the resealing suggested that SLO is removed instead of disassembled (Idone et al., 2008). To determine if SLO pores were removed from the plasma membrane by endocytosis, the researchers used membrane-impermeable fluorescent dextran, which assesses endosomal formation, on cells with SLO (Idone et al., 2008). Dextran was subsequently detected in many endosomes of the cells when in the presence of Ca^{2+}, thereby signifying membrane wounding (Idone et al., 2008). Without Ca^{2+}, sealing did not occur and the tracer could easily be found within the cells (Idone et al., 2008). Further, without SLO, the tracer was barely visible within the cells (Idone et al., 2008). As membrane resealing with SLO occurs in less than 30 seconds, the investigators wanted to determine if the kinetics of endocytosis coincided with this period (Idone et al., 2008). HeLa cells were therefore labeled with a glycolipid anchored green fluorescent protein, YFP-GPI adenovirus construct, and imaged (Idone et al., 2008). Vesicles containing YFP-GPI were found inside cells 5 to 15 seconds after introduction of SLO (Idone et al., 2008). There was little YFP-GPI to be found within the cells without SLO (Idone et al., 2008). These observations suggested that cholesterol may play a role in

endocytosis. The researchers thus performed cholesterol extraction with methyl-β-cyclodextrin and found dose-dependent reduction of endocytosis and membrane resealing (Idone et al., 2008). Idone and colleagues (2008) ultimately concluded that endocytosis is an important defense mechanism against pore-forming proteins, and may participate in the resealing of mechanical injuries.

Following the previous study, Tam and colleagues (2010) investigated the role of acid sphingomyelinase and lysosomal exocytosis in plasma membrane repair. The researchers used a method to inhibit lysosomal exocytosis without the removal of Ca^{2+} from the extracellular medium (Tam et al., 2010). This is particularly important because membrane repair is strongly Ca^{2+}-dependent and maintaining physiologically relevant conditions provides better control over possible extraneous factors (Tam et al., 2010). The researchers used bromoenol lactone (BEL) to strongly inhibit the extracellular aggregation of lysosomal β-hexosaminidase when exposed to SLO (Tam et al., 2010). The result of the BEL-treated cells showed a 10-fold reduction of endosomes and impaired resealing when exposed to SLO (Tam et al., 2010). To investigate the possible role of ASM in membrane repair, the researchers exposed cells to either Ca^{2+} or Mg^{2+}, and with or without SLO. They found a dramatic increase in ASM activity when cells were exposed to SLO and Ca^{2+} (Tam et al., 2010). No changes were observed when cells were treated with Mg^{2+} and SLO (Tam et al., 2010). Similarly, no changes were observed when SLO was absent (Tam et al., 2010). The researchers also investigated the requirement of ASM for endocytosis using desipramine (DPA), a strong ASM inhibitor (Tam et al., 2010). NRK cells treated with DPA demonstrated 95% reduction in ASM activity and 50% reduction in endosomes, but showed no other lysosome exocytosis when exposed to SLO in the presence of Ca^{2+} (Tam

et al., 2010). Using FM1-43 staining to assess membrane resealing, the results showed DPA-treated cells impaired membrane resealing compared to untreated cells (Tam et al., 2010). These findings suggest that ASM has a role in endocytosis and that lysosomal exocytosis is insufficient to fully repair the plasma membrane (Tam et al., 2010). Using human lymphoblasts from a patient with NPD/A, the investigators also observed impaired membrane resealing after exposure to SLO in the presence of Ca^{2+} (Tam et al., 2010). Similar findings were reported with human fibroblasts taken from a patient with NPD/A (Tam et al., 2010). Impaired membrane repair was similarly found in transcriptionally silenced *SMPD1*, a gene encoding for ASM, in HeLa cells (Tam et al., 2010). The addition of recombinant human ASM (rhASM) to these cells restored endocytosis and membrane resealing (Tam et al., 2010). With these findings, Tam and colleagues (2010) were therefore able to demonstrate the necessity for exocytosis of ASM in endocytosis and plasma membrane repair.

Corrotte and colleagues (2013) added to the results of the previous study by investigating caveolae internalization as a mechanism for membrane repair in wounded cells and muscle fibers. In their study, NRK cells were exposed to green fluorescent protein (GFP)-tagged SLO and results showed a disappearance of GFP-SLO from the plasma membrane over time (Corrotte et al., 2013). Additionally, GFP-SLO detection on internalized vesicles containing caveolin-1 (Cav1) slowly increased over the first 60 seconds (Corrotte et al., 2013). By 300 seconds, small vesicles (<80 nm) containing Cav1, or both Cav1 and SLO, decreased while larger vesicles (>80 nm) increased, which suggests a merging of the endocytic compartments (Corrotte et al., 2013). Using FM1-43 to visualize membrane permeability, it was then found that the cells with Cav1 silencing were

permeable when treated with SLO in presence of Ca^{2+}, thereby suggesting a dysfunction in membrane repair (Corrotte et al., 2013). Corrotte and colleagues (2013) also evaluated caveolae internalization during resealing of mechanical wounding, which were induced with glass beads. Wounded cells treated with Cav1 siRNA in the presence of Ca^{2+} showed greater PI staining than controls suggesting the disruption of membrane repair after inhibition of Cav1 (Corrotte et al., 2013). The investigators further explored caveolae formation and membrane repair in C2C12 myoblasts and myotubes, and found that myotubes treated with SLO or sphingomyelinase generated an increasing number of small caveolae-like vesicles within a 30 second period (Corrotte et al., 2013). In particular, their study used caveolin-3 (Cav3) silenced myotubes in order to show the importance of Cav3 in membrane repair (Corrotte et al., 2013). These myotubes showed a high level of nuclear PI staining, thus indicating membrane injury when exposed to SLO and Ca^{2+} (Corrotte et al., 2013). No nuclear staining was detected in myotubes without SLO or Ca^{2+}, therefore indicating an intact membrane. Corrotte and colleagues (2013) evaluated membrane repair in single muscle fibers (SMFs) of the mouse flexor digitorum brevis (FDB) as well. Their results showed that in the absence of Ca^{2+}, SLO induced PI staining of the nuclei in the muscle fibers (Corrotte et al., 2013). However, with Ca^{2+}, there was no PI influx, suggesting proper resealing of the sarcolemma (Corrotte et al., 2013). Additionally, mechanical wounding of muscle fibers during dissection demonstrated an accumulation of caveolae-like compartments located near the damaged sarcolemma (Corrotte et al., 2013). The study by Corrotte and colleagues (2013) thus strongly supports the role of caveolar endocytosis as a critical component to plasma membrane integrity and repair.

5.6 – Mechanisms of fatigue in skeletal muscle

Muscle fatigue is defined as the inability of the muscle to generate force, which occurs when skeletal muscle undergoes repeated stimulation resulting in a reduction in function (Westerblad & Allen, 1991). Several mechanisms have been proposed to influence fatigue, e.g., the accumulation of metabolites, depletion of substrates, reduced Ca^{2+} release, and reduced Ca^{2+} sensitivity of the myofilaments (Danieli-Betto, Germinario, Esposito, Biral, & Betto, 2000); however, findings have been quite variable. It is worth noting that results from some studies are limited in their use because of non-physiological concentrations of ions and metabolites (Allen, 2009). However, other studies have findings that better represent physiological conditions.

Investigations into the effects of fatigue on force production began in the 1970s. Edwards and colleagues (1977) reported differences in the ability of the muscle to respond to low and high stimulation frequencies after subjected to fatiguing contractions. They found that muscular force generation at high frequency after fatigue was diminished for about 20 minutes, but force production at low frequency stimulation was further diminished for more than a day (Edwards et al., 1977). Moreover, the investigators assessed changes in force production between muscles subjected to low or high frequency stimulation during fatigue (Edwards et al., 1977). Their findings revealed that the decline in force was greater during low frequency stimulation than high frequency stimulation (Edwards et al., 1977). Furthermore, the decline in force during low frequency stimulation was not ascribed to electrical activity failure or to a reduction in high-energy phosphate levels (Edwards et al., 1977).

Following the previous study, Dawson and colleagues (1980) simultaneously used force measurements as well as phosphorus nuclear magnetic resonance in order to correlate the changes in muscle function to biochemical fluctuations. In particular, the investigators measured several different variables in the gastrocnemius subjected to fatigue (Dawson, et al., 1980). Specifically, they assessed isometric force production, ATP hydrolysis, and concentrations of creatine phosphate (CrP), creatine (Cr), ATP, adenosine diphosphate (ADP), inorganic phosphate (P_i), and hydrogen ions (H^+) (Dawson et al., 1980). They found that the mechanical changes, decline in force generation, and slower rate of relaxation were correlated with the metabolic changes during muscular fatigue (Dawson et al., 1980). Dawson and colleagues (1980) suggested that some metabolites, such as Cr, CrP, and ATP, may have contributed to the reduction in the rate of relaxation. They further postulated that the decline in ATP hydrolysis during fatiguing stimulation was a result of greater product concentration rather than a decline in ATP concentration (Dawson et al., 1980). Finally, Dawson and colleagues (1980) posited that the relationship between the rate of relaxation and ATP hydrolysis could be associated with SR-Ca^{2+} sequestration. Unfortunately, the investigators did not assess SR-Ca^{2+} uptake in this study. Dawson and colleagues (1980) were nonetheless able to link biochemical changes with fatigue leading to better insight into factors contributing to muscular force decline.

Skeletal muscle fatigue can also be assessed in isolated fibers from murine FDB. Westerblad and Lännergren (1987) exposed SMFs to fatigue and assessed time to fatigue and force decline. They also explored the effects of acidosis and caffeine on force recovery (Westerblad and Lännergren, 1987). Their fatigue protocol employed electrical stimulation of SMFs with repeated tetani at 70Hz once every 3.8s for 2 minutes

(Westerblad and Lännergren, 1987). Depending on the condition of the fiber, they continued to reduce the resting time between contractions until the fiber reached fatigue, which they defined as 30% of initial force (Westerblad & Lännergren, 1987). The investigators ultimately found that there was great variability in the fatigue resistance of SMFs (2.5 to 25 minutes), with most fibers reaching fatigue between 4 to 8 minutes (Westerblad & Lännergren, 1987). Their findings further revealed that caffeine had no effect on force production during rest, but produced stark rises in tension when applied after fatigue (Westerblad & Lännergren, 1987). The investigators also observed decreased time to fatigue when they subjected SMFs to increasing levels of acidosis. Of note, administration of caffeine to these same fibers resulted in some recovery (Westerblad & Lännergren, 1987). Westerblad & Lännergren (1987) subsequently concluded that there were three different phases of muscle fatigue: phase 1) tetanic force decline to 85% of its initial measurement; phase 2) plateau in force production; and, phase 3) rapid force decline. They thus surmised that the decline in force in phases 1 and 3 of fatigue had separate underlying intracellular mechanisms.

Westerblad and Allen (1991) thereafter completed a study using Fura-2, a Ca^{2+} indicator, to measure $[Ca^{2+}]_i$ in SMFs during fatigue. This was the first investigation to concurrently measure tension and use Fura-2 to assess $[Ca^{2+}]_i$ in mammalian SMFs. Their results revealed an increase in resting $[Ca^{2+}]_i$ with the progression of repeated tetanic contractions (Westerblad & Allen, 1991). They found that administering caffeine could not rescue early tension decline (Westerblad & Allen, 1991). This latter finding suggested that metabolic alterations could have influenced force production during the first phase of fatigue (Westerblad & Allen, 1991). In any event, either intracellular acidosis or a rise in

P_i levels could have contributed to the rapid decline to 90% of the initial tension (Westerblad & Allen, 1991). In terms of the rapid force decline during the third phase, the investigators suggested that a reduction in intracellular Ca^{2+} could have compromised the activation of cross-bridges (Westerblad & Allen, 1991). To support this, Westerblad and Allen (1991) used caffeine to raise tetanic intracellular Ca^{2+} levels and rescue force to 80% of its initial measure.

Later, in the mid-1990s, several groups studied the mechanisms contributing to Ca^{2+} release, Ca^{2+} sensitivity of myofibrillar proteins, and the effects of pH fluctuation during fatigue. For example, findings by Fryer and colleagues (1995) and Owen and colleagues (1996) suggested that decreased Ca^{2+} release could be due to metabolic and non-metabolic factors. Around the same time, some studies demonstrated that pH could play a role in SR-Ca^{2+} release (Favero et al., 1995), while others reported no effect (Westerblad & Allen, 1992). Of note, these studies all used different methods to assess SR-Ca^{2+} release, possibly leading to the difference in findings. These discrepancies thus limit the conclusions of physiological mechanisms underlying muscle fatigue.

Of particular relevance, Chin and Allen (1998) suggested that the pH fluctuations in muscle fatigue was dependent on fiber type and intensity. The researchers assessed the differences in force, $[Ca^{2+}]_i$, and pH in SMFs exposed to fatigue protocols of different intensities (Chin & Allen, 1998). Both fatiguing conditions involved stimulation of SMFs at 100Hz; however, the protocols differed with regard to the time between successive stimulations (Chin & Allen, 1998). The standard fatigue protocol begins with stimulation initiated once every 4 seconds for 2 minutes, after which the intermittent period is decreased by 1 second every 2-minute interval until the force production of the fiber is

30% of the initial force (Chin & Allen, 1998). The protocols in this study kept consistent intermittent periods, either in the form of tetani every 1 second or every 4 seconds, until reaching 30% initial force (Chin & Allen, 1998). Fibers undergoing stimulation every 4 seconds were said to be exposed to low intensity tetani, while fibers undergoing the 1-second variation were high intensity tetani (Chin & Allen, 1998). Fibers that underwent the high intensity tetani reached 30% of initial force quicker than fibers that underwent the low intensity tetani (Chin & Allen, 1998). Yet, the reduction in $[Ca^{2+}]_i$ was greater in SMFs subjected to low intensity tetani (48%) than those subjected to high intensity tetani (35%) (Chin & Allen, 1998). The rapid decline in force at high intensity tetani attributed to Ca^{2+} release failure (Chin & Allen, 1998). When the fibers reached 30% of its initial force, SMFs were treated with 5mM caffeine, which is a Ca^{2+} release channel agonist (Chin & Allen, 1998). Caffeine was able to restore force in SMFs exposed to fatigue at low intensity tetani, but the same did not occur with high intensity tetani (Chin & Allen, 1998). This suggested that the decline in Ca^{2+} release during fatigue from high intensity tetani is likely related to inadequate SR-Ca^{2+} reuptake. The investigators also assessed pH changes in low and high intensity fatigue (Chin & Allen, 1998). Specifically, they found that high intensity fatigue brought about greater and quicker increase in acidosis (Chin & Allen, 1998). These findings show that Ca^{2+} sensitivity is diminished when muscles are subjected to increased levels of acidosis (Chin & Allen, 1998).

Danieli-Betto and colleagues (2000) also investigated if fatigue-induced modifications of the SR and myofibrillar proteins led to reduction of tension in mammalian muscle fibers. In their study, the investigators used skinned muscle fiber technique to assess SR-Ca^{2+} release and uptake, SR caffeine sensitivity, and myofibrillar protein Ca^{2+}

sensitivity in both fast- and slow-twitch fibers (Danieli-Betto et al., 2000). They found that maximal Ca^{2+} tension was not different between fatigued and rested fibers, indicating that fatigue-induced changes in Ca^{2+} sensitivity were due to alterations in the myofibrillar proteins (Danieli-Betto et al., 2000). Additionally, there was a more rapid accumulation of Ca^{2+} in the SR of slow-twitch muscle fibers when skinned immediately after fatigue than those skinned before fatigue (Danieli-Betto et al., 2000). Moreover, the SR-Ca^{2+} release behavior in both slow- and fast-twitch skinned fibers persisted after fatigue (Danieli-Betto et al., 2000). Conversely, intact SMFs had slower rates of Ca^{2+} removal (Danieli-Betto et al., 2000). The authors suggested that this was due to increased levels of metabolites, posttranslational modification of the SR-Ca^{2+} pump, and/or phospholamban activity. Finally, Danieli-Betto and colleagues (2000) posited that alterations to the SR and myofibrillar proteins are at least partially responsible for the fatigue-induced force decline in slow-twitch fibers, but not in fast-twitch fibers.

High rises in $[Ca^{2+}]_i$ can also bring about decline in tension during fatigue. Muscle excitation induces the release of Ca^{2+} into the myoplasm, increasing $[Ca^{2+}]_i$ from 50nM to 1-2μM (Westerblad & Allen, 1991). Previous studies suggested that elevated $[Ca^{2+}]_i$ played a role in the development of persisted fatigue; however, prior studies did not investigate if peak Ca^{2+} levels or temporal accumulation of Ca^{2+} disrupted E-C coupling (Chin & Allen, 1996; Lamb, Junankar, & Stephenson, 1995; Westerblad & Allen, 1993). To answer this question, Verburg and colleagues (2006) manipulated Ca^{2+} levels in mechanically skinned fibers to assess the effects on E-C uncoupling. Their findings showed that E-C uncoupling in fast-twitch fibers occurred when $[Ca^{2+}]_i$ was raised by 2μM for a minute or more (Verburg et al., 2006). Their findings further suggested that peak

Ca^{2+}, rather than the temporal accumulation of Ca^{2+}, was responsible for E-C uncoupling. Additionally, uncoupling was only apparent when peak Ca^{2+} levels occurred near the triad junction rather than the center of the myoplasm (Verburg et al., 2006). Therefore, signal transduction failure at the triad junction was found to be the primary culprit in E-C coupling disruption (Verburg et al., 2006).

Roots and colleagues (2009) thereafter investigated fatigue following repeated short isometric contractions and repeated concentric contractions at temperatures of 10°C, 20°C, and 30°C. Repeated concentric contractions produced greater decline in force than isometric contractions (Roots et al., 2009). Isometric contractions during fatigue resulted in less force decline at 30°C (20%) than 10°C (30%) (Roots et al., 2009). Additionally, absolute power rose by more than ten-fold from 10°C to 30°C (Roots et al., 2009). The results of Roots and colleagues (2009) thus suggested that the decline in power after fatigue was greater at 10°C than at higher temperatures. Roots and colleagues (2009) subsequently demonstrated that muscle fatigue is temperature sensitive and that skeletal muscle does not perform optimally at lower temperatures.

5.7 – Role of Ca^{2+} deprivation on E-C coupling and fatigue

Ca^{2+} ions play a critical role in the coupling of electrical and mechanical events of skeletal muscle. Inside a muscle fiber, Ca^{2+} binds to troponin, allowing troponin to remove tropomyosin from the myosin-binding site on actin, thereby permitting cross-bridge cycling and force production (Ashley et al., 1992). Ca^{2+} also plays a role in membrane potential in the extracellular space surrounding a muscle fiber. In particular, Curtis (1963) excised the extensor longus digiti IV muscle of the English and American frog and

immersed them in a choline-Ringer's solution (1.8mM $CaCl_2$), followed by a Ca^{2+}-free Ringer's solution (0 mM $CaCl_2$). Electrodes were then inserted into the muscle, and resting potentials were measured using a cathode-ray oscilloscope (Curtis, 1963). Contraction was next induced using potassium chloride (KCl). A capacity strain gauge or RCA 5734 transducer was used to measure force production. Curtis (1963) subsequently observed a decline in membrane potential when transferring the muscle from the choline-Ringer's solution to the Ca^{2+}-free Ringer's solution as the average membrane potential in choline-Ringer's solution was about 80mV compared to 65mV in Ca^{2+}-free Ringer's solution (Curtis, 1963). There was little to no potassium (K^+) induced contraction after 15 minutes in the Ca^{2+}-free Ringer's solution (Curtis, 1963). As such, Curtis (1963) concluded that removal of Ca^{2+} had a direct effect on tension response through alteration in membrane potential.

A similar, yet separate, study was performed by Jenden and Reger (1963) to examine the role of falling resting potential in the failure of electrically stimulated contraction. Their study used dissected sartorius muscle of the common frog and mounted it to a RCA 5734 transducer (Jenden & Reger, 1963). A set of electrodes were then used to measure membrane potential, while another set was inserted into the muscle fibers for electrical stimulation (Jenden & Reger, 1963). When muscle fibers were exposed to a Ca^{2+}-free Ringer's solution (0mM $CaCl_2$ and 0.2mM EDTA), membrane potential decreased to 65-70mV, thus correlating with a loss of mechanical response (Jenden & Reger, 1963). Only a portion of the unresponsive fibers recovered to new stimulation when Ca^{2+} was restored (Jenden & Reger, 1963). The measured resistance during Ca^{2+} deprivation (~277kΩ) and Ca^{2+} restoration (~271kΩ) was no different. Replacement of

Ca^{2+} with magnesium, manganese, strontium, nickel, and cobalt, were all able to maintain normal membrane potential and contraction (Jenden & Reger, 1963). Although Jenden & Reger (1963) attempted to hyperpolarize unresponsive fibers in Ca^{2+}-free solution by manipulating the current to the stimulating electrode, they were only able to induce a localized contraction. The investigators therefore concluded that the effects of calcium deprivation on mechanical responsiveness to electrical stimulation were the result of the decreased resting potential (Jenden & Reger, 1963).

Contrary to previous studies, Dulhunty & Gage (1988) observed how extracellular calcium and dihydropyridines affected contraction in rat soleus muscle fibers by employing electrical and K^+ induced stimulations in fibers exposed to Ringer's solution varying in Ca^{2+} concentrations (0, 3, and 85µM Ca^{2+}) (Dulhunty & Gage, 1988). Electrical stimulation and K^+ induced similar contractions. However, subsequent contractions produced diminishing force, and K^+ contractions decayed at a faster rate than electrical stimulation (Dulhunty & Gage, 1988). Full recovery was observed within 10-15 minutes of exposure to a solution with 2.5mM Ca^{2+}. Fibers exposed to a 2.5mM Ca^{2+} solution containing nifedipine (50µM), a DHPR inhibitor, was still able to contract and with greater force than fibers exposed to low Ca^{2+} solutions (Dulhunty & Gage, 1988). Both the solution with nifedipine as well as the low Ca^{2+} solutions induced similar decaying contractions in fibers (Dulhunty & Gage, 1988). Based on said results, Dulhunty & Gage (1988) conjectured that the binding or dissociation of Ca^{2+} from a dihydropyridine-binding molecule located in the walls of the T-tubule may have mediated these effects.

Prior studies have largely investigated removal of Ca^{2+} and its effect on E-C coupling during contraction. These studies have not explored Ca^{2+} removal and its effect

on E-C coupling during fatigue. Of particular relevance, Williams (1990) performed a study to investigate the effects of low extracellular Ca^{2+} and Ca^{2+} antagonists (e.g. diltiazem and D-600) on skeletal muscle fatigue. The investigator excised the sartorius muscles from male northern leopard frogs and mounted them on a force transducer (Williams, 1990). Low Ca^{2+} Ringer's solution was created by substituting $CaCl_2$ with 3mM $MgCl_2$ and 1mM EGTA (Williams, 1990). Ditiazem and D-600 were added separately to their respective Ringer's solution to achieve a concentration of 30μM (Williams, 1990). The relevant muscles were then incubated in each of the three aforementioned Ringer's solutions and exposed to repetitive twitch stimulation of 1Hz for 15 minutes each (Williams, 1990). The Ca^{2+} antagonists increased both the rate and magnitude of fatigue compared to control (normal Ringer's solution); however, the low Ca^{2+} Ringer's solution only slightly increased the rate of fatigue (Williams, 1990). Following these bouts of fatigue, K^+ (180mM) or caffeine (10mM) were added to incubation media to induce contracture (Williams, 1990). Caffeine was able to elicit contraction in all muscles, but K^+ was only able to elicit contraction in the control muscles (Williams, 1990). Williams (1990) later suggested that extracellular Ca^{2+} influx through voltage-dependent Ca^{2+} channels may have some influence on skeletal muscle during prolonged repetitive twitch.

5.8 – Summary

Niemann-Pick disease (NPD) is a lysosomal storage disorder that can affect a wide variety of body systems to varying degrees of severity (Gumbinas et al., 1975; Meikle et al., 1999; Mendelson et al., 2006). Although the main cause of NPD types A (NPD/A) and B (NPD/B) is acid sphingomyelinase deficiency as a result of *SMPD1* mutation (Goñi &

Alonso, 2002; Jenkins et al., 2009), the underlying mechanisms contributing to muscle weakness are not well understood. ASM deficiency has been implicated in the impairment of membrane repair (Tam et al., 2010; Corrotte et al., 2013), and skeletal muscle fibers regularly undergo the process of damage and repair (Chargé et al., 1984); therefore, investigations into the mouse model of NPD/A, ASM-/-, may potentially better our understanding of the relationship between plasma membrane repair and E-C coupling.

More specifically, we believe there may be a link between the impaired membrane repair mechanism and E-C uncoupling in ASM-/- fibers. In ASM-/- fibers, ASM deficiency prevents caveolae formation, thereby leaving the damaged membrane unrepaired (Corrotte et al., 2013). Similarly, when wounded cells are deprived of extracellular Ca^{2+} using EGTA, exocytosis of lysosomes and membrane repair is inhibited (Reddy et al., 2001). Both ASM deficiency and removal of extracellular Ca^{2+} fail to trigger membrane repair. Moreover, extracellular Ca^{2+} removal has been shown to diminish skeletal muscle force production (Curtis, 1963; Dulhunty & Gage, 1988; Jenden & Reger, 1963; Williams, 1990). E-C uncoupling may be exacerbated during prolonged repeated contractions (Lamb, 2009), and may manifest as muscle weakness in ASM-/- mice. Given the observed membrane repair impairment in ASM deficiency and extracellular Ca^{2+} absence and the reduced force production without Ca^{2+}, we believe that that we may be able to establish a correlation between membrane repair disruption and E-C uncoupling in ASM-/- mice.

Appendix

Three-way ANOVA at 0Hz

Within-Subjects Factors

Measure: MEASURE_1

Time	Dependent Variable
1	BL
2	t30
3	t60

Between-Subjects Factors

		Value Label	N
Genotype	1.00	WT	19
	2.00	ASM-/-	18
Treatment	1.00	Calcium	17
	2.00	EGTA	20

Descriptive Statistics

	Genotype	Treatment	Mean	Std. Deviation	N
BL	WT	Calcium	.3081	.09034	9
		EGTA	.2635	.01638	10
		Total	.2846	.06546	19
	ASM-/-	Calcium	.2734	.04375	8
		EGTA	.2780	.01517	10
		Total	.2759	.03026	18

	Total	Calcium	.2918	.07237	17
		EGTA	.2708	.01707	20
		Total	.2804	.05093	37
t30	WT	Calcium	.3142	.09144	9
		EGTA	.2675	.02594	10
		Total	.2896	.06802	19
	ASM-/-	Calcium	.2785	.05853	8
		EGTA	.2741	.02287	10
		Total	.2761	.04114	18
	Total	Calcium	.2974	.07757	17
		EGTA	.2708	.02404	20
		Total	.2830	.05622	37
t60	WT	Calcium	.3130	.09146	9
		EGTA	.2685	.03209	10
		Total	.2896	.06895	19
	ASM-/-	Calcium	.3170	.11433	8
		EGTA	.2788	.03141	10
		Total	.2958	.07929	18
	Total	Calcium	.3149	.09953	17
		EGTA	.2737	.03136	20
		Total	.2926	.07318	37

Multivariate Tests[a]

Effect		Value	F	Hypothesis df	Error df	Sig.	Partial Eta Squared
Time	Pillai's Trace	.073	1.254[b]	2.000	32.000	.299	.073
	Wilks' Lambda	.927	1.254[b]	2.000	32.000	.299	.073
	Hotelling's Trace	.078	1.254[b]	2.000	32.000	.299	.073
	Roy's Largest Root	.078	1.254[b]	2.000	32.000	.299	.073
Time * Genotype	Pillai's Trace	.095	1.674[b]	2.000	32.000	.204	.095
	Wilks' Lambda	.905	1.674[b]	2.000	32.000	.204	.095
	Hotelling's Trace	.105	1.674[b]	2.000	32.000	.204	.095
	Roy's Largest Root	.105	1.674[b]	2.000	32.000	.204	.095
Time * Treatment	Pillai's Trace	.046	.764[b]	2.000	32.000	.474	.046
	Wilks' Lambda	.954	.764[b]	2.000	32.000	.474	.046
	Hotelling's Trace	.048	.764[b]	2.000	32.000	.474	.046
	Roy's Largest Root	.048	.764[b]	2.000	32.000	.474	.046
Time * Genotype * Treatment	Pillai's Trace	.049	.827[b]	2.000	32.000	.446	.049
	Wilks' Lambda	.951	.827[b]	2.000	32.000	.446	.049
	Hotelling's Trace	.052	.827[b]	2.000	32.000	.446	.049
	Roy's Largest Root	.052	.827[b]	2.000	32.000	.446	.049

Three-way ANOVA at 10Hz

Within-Subjects Factors

Measure: MEASURE_1

Time	Dependent Variable
1	BL
2	t30
3	t60

Between-Subjects Factors

		Value Label	N
Genotype	1.00	WT	19
	2.00	ASM-/-	17
Treatment	1.00	Calcium	16
	2.00	EGTA	20

Descriptive Statistics

	Genotype	Treatment	Mean	Std. Deviation	N
BL	WT	Calcium	.6118	.07449	9
		EGTA	.5316	.08184	10
		Total	.5696	.08664	19
	ASM-/-	Calcium	.4947	.05949	7
		EGTA	.5783	.12245	10
		Total	.5439	.10751	17
	Total	Calcium	.5606	.08929	16

		EGTA	.5550	.10416	20
		Total	.5574	.09651	36
t30	WT	Calcium	.5883	.04220	9
		EGTA	.5691	.04561	10
		Total	.5782	.04392	19
	ASM-/-	Calcium	.5526	.08220	7
		EGTA	.5668	.12709	10
		Total	.5609	.10803	17
	Total	Calcium	.5727	.06315	16
		EGTA	.5680	.09294	20
		Total	.5701	.08002	36
t60	WT	Calcium	.5699	.04871	9
		EGTA	.5587	.05977	10
		Total	.5640	.05361	19
	ASM-/-	Calcium	.5530	.12458	7
		EGTA	.5302	.10205	10
		Total	.5396	.10868	17
	Total	Calcium	.5625	.08688	16
		EGTA	.5445	.08270	20
		Total	.5525	.08385	36

Multivariate Tests[a]

Effect	Value	F	Hypothesis df	Error df	Sig.	Partial Eta Squared

Time	Pillai's Trace	.104	1.808[b]	2.000	31.000	.181	.104
	Wilks' Lambda	.896	1.808[b]	2.000	31.000	.181	.104
	Hotelling's Trace	.117	1.808[b]	2.000	31.000	.181	.104
	Roy's Largest Root	.117	1.808[b]	2.000	31.000	.181	.104
Time * Genotype	Pillai's Trace	.009	.143[b]	2.000	31.000	.867	.009
	Wilks' Lambda	.991	.143[b]	2.000	31.000	.867	.009
	Hotelling's Trace	.009	.143[b]	2.000	31.000	.867	.009
	Roy's Largest Root	.009	.143[b]	2.000	31.000	.867	.009
Time * Treatment	Pillai's Trace	.020	.318[b]	2.000	31.000	.730	.020
	Wilks' Lambda	.980	.318[b]	2.000	31.000	.730	.020
	Hotelling's Trace	.021	.318[b]	2.000	31.000	.730	.020
	Roy's Largest Root	.021	.318[b]	2.000	31.000	.730	.020
Time * Genotype * Treatment	Pillai's Trace	.169	3.150[b]	2.000	31.000	.057	.169
	Wilks' Lambda	.831	3.150[b]	2.000	31.000	.057	.169
	Hotelling's Trace	.203	3.150[b]	2.000	31.000	.057	.169
	Roy's Largest Root	.203	3.150[b]	2.000	31.000	.057	.169

Three-way ANOVA at 30Hz

Within-Subjects Factors

Measure: MEASURE_1

Time	Dependent Variable
1	BL
2	t30
3	t60

Between-Subjects Factors

		Value Label	N
Genotype	1.00	WT	19
	2.00	ASM-/-	17
Treatment	1.00	Calcium	16
	2.00	EGTA	20

Descriptive Statistics

	Genotype	Treatment	Mean	Std. Deviation	N
BL	WT	Calcium	.8670	.09590	9
		EGTA	.7265	.13915	10
		Total	.7931	.13771	19
	ASM-/-	Calcium	.6619	.11041	7
		EGTA	.7945	.17451	10
		Total	.7399	.16195	17
	Total	Calcium	.7773	.14432	16

		EGTA	.7605	.15752	20
		Total	.7679	.14989	36
t30	WT	Calcium	.8502	.06835	9
		EGTA	.7980	.08644	10
		Total	.8227	.08081	19
	ASM-/-	Calcium	.7487	.11323	7
		EGTA	.7905	.21623	10
		Total	.7733	.17764	17
	Total	Calcium	.8058	.10161	16
		EGTA	.7943	.16032	20
		Total	.7994	.13569	36
t60	WT	Calcium	.8093	.08316	9
		EGTA	.7905	.07189	10
		Total	.7994	.07584	19
	ASM-/-	Calcium	.7350	.13062	7
		EGTA	.7231	.17734	10
		Total	.7280	.15532	17
	Total	Calcium	.7768	.10937	16
		EGTA	.7568	.13616	20
		Total	.7657	.12367	36

Multivariate Tests[a]

Effect	Value	F	Hypothesis df	Error df	Sig.	Partial Eta Squared

Time	Pillai's Trace	.189	3.618[b]	2.000	31.000	.039	.189
	Wilks' Lambda	.811	3.618[b]	2.000	31.000	.039	.189
	Hotelling's Trace	.233	3.618[b]	2.000	31.000	.039	.189
	Roy's Largest Root	.233	3.618[b]	2.000	31.000	.039	.189
Time * Genotype	Pillai's Trace	.013	.210[b]	2.000	31.000	.812	.013
	Wilks' Lambda	.987	.210[b]	2.000	31.000	.812	.013
	Hotelling's Trace	.014	.210[b]	2.000	31.000	.812	.013
	Roy's Largest Root	.014	.210[b]	2.000	31.000	.812	.013
Time * Treatment	Pillai's Trace	.004	.068[b]	2.000	31.000	.935	.004
	Wilks' Lambda	.996	.068[b]	2.000	31.000	.935	.004
	Hotelling's Trace	.004	.068[b]	2.000	31.000	.935	.004
	Roy's Largest Root	.004	.068[b]	2.000	31.000	.935	.004
Time * Genotype * Treatment	Pillai's Trace	.167	3.111[b]	2.000	31.000	.059	.167
	Wilks' Lambda	.833	3.111[b]	2.000	31.000	.059	.167
	Hotelling's Trace	.201	3.111[b]	2.000	31.000	.059	.167
	Roy's Largest Root	.201	3.111[b]	2.000	31.000	.059	.167

Three-way ANOVA at 50Hz

Within-Subjects Factors

Measure: MEASURE_1

Time	Dependent Variable
1	BL
2	t30
3	t60

Between-Subjects Factors

		Value Label	N
Genotype	1.00	WT	19
	2.00	ASM-/-	16
Treatment	1.00	Calcium	16
	2.00	EGTA	19

Descriptive Statistics

	Genotype	Treatment	Mean	Std. Deviation	N
BL	WT	Calcium	1.0508	.17233	9
		EGTA	.8512	.19653	10
		Total	.9457	.20735	19
	ASM-/-	Calcium	.7537	.15453	7
		EGTA	.8728	.21876	9
		Total	.8207	.19697	16
	Total	Calcium	.9208	.22035	16

		EGTA	.8614	.20175	19
		Total	.8886	.20946	35
t30	WT	Calcium	1.0091	.12557	9
		EGTA	.9481	.12592	10
		Total	.9770	.12616	19
	ASM-/-	Calcium	.9170	.17651	7
		EGTA	.9046	.28541	9
		Total	.9100	.23653	16
	Total	Calcium	.9688	.15198	16
		EGTA	.9275	.21126	19
		Total	.9464	.18508	35
t60	WT	Calcium	.9860	.18410	9
		EGTA	.9546	.12784	10
		Total	.9695	.15328	19
	ASM-/-	Calcium	.8846	.16148	7
		EGTA	.8268	.22381	9
		Total	.8521	.19499	16
	Total	Calcium	.9416	.17665	16
		EGTA	.8941	.18637	19
		Total	.9158	.18093	35

Multivariate Tests[a]

Effect	Value	F	Hypothesis df	Error df	Sig.	Partial Eta Squared

Time	Pillai's Trace	.131	2.268[b]	2.000	30.000	.121	.131
	Wilks' Lambda	.869	2.268[b]	2.000	30.000	.121	.131
	Hotelling's Trace	.151	2.268[b]	2.000	30.000	.121	.131
	Roy's Largest Root	.151	2.268[b]	2.000	30.000	.121	.131
Time * Genotype	Pillai's Trace	.058	.931[b]	2.000	30.000	.405	.058
	Wilks' Lambda	.942	.931[b]	2.000	30.000	.405	.058
	Hotelling's Trace	.062	.931[b]	2.000	30.000	.405	.058
	Roy's Largest Root	.062	.931[b]	2.000	30.000	.405	.058
Time * Treatment	Pillai's Trace	.001	.019[b]	2.000	30.000	.982	.001
	Wilks' Lambda	.999	.019[b]	2.000	30.000	.982	.001
	Hotelling's Trace	.001	.019[b]	2.000	30.000	.982	.001
	Roy's Largest Root	.001	.019[b]	2.000	30.000	.982	.001
Time * Genotype * Treatment	Pillai's Trace	.167	3.003[b]	2.000	30.000	.065	.167
	Wilks' Lambda	.833	3.003[b]	2.000	30.000	.065	.167
	Hotelling's Trace	.200	3.003[b]	2.000	30.000	.065	.167
	Roy's Largest Root	.200	3.003[b]	2.000	30.000	.065	.167

Three-way ANOVA at 70Hz

Within-Subjects Factors

Measure: MEASURE_1

Time	Dependent Variable
1	BL
2	t30
3	t60

Between-Subjects Factors

		Value Label	N
Genotype	1.00	WT	17
	2.00	ASM-/-	15
Treatment	1.00	Calcium	14
	2.00	EGTA	18

Descriptive Statistics

	Genotype	Treatment	Mean	Std. Deviation	N
BL	WT	Calcium	1.1743	.19215	8
		EGTA	.8718	.16823	9
		Total	1.0141	.23350	17
	ASM-/-	Calcium	.7997	.19878	6
		EGTA	.9687	.24996	9
		Total	.9011	.23908	15
	Total	Calcium	1.0137	.26848	14

		EGTA	.9202	.21262	18
		Total	.9611	.23925	32
t30	WT	Calcium	1.1879	.15025	8
		EGTA	1.0451	.15410	9
		Total	1.1123	.16476	17
	ASM-/-	Calcium	.9622	.24062	6
		EGTA	1.0088	.34682	9
		Total	.9901	.29995	15
	Total	Calcium	1.0911	.21877	14
		EGTA	1.0269	.26102	18
		Total	1.0550	.24182	32
t60	WT	Calcium	1.1436	.15088	8
		EGTA	1.0620	.15049	9
		Total	1.1004	.15181	17
	ASM-/-	Calcium	1.0207	.20901	6
		EGTA	.8973	.26278	9
		Total	.9467	.24284	15
	Total	Calcium	1.0909	.18179	14
		EGTA	.9797	.22434	18
		Total	1.0283	.21120	32

Multivariate Tests[a]

Effect	Value	F	Hypothesis df	Error df	Sig.	Partial Eta Squared

Time	Pillai's Trace	.160	2.573[b]	2.000	27.000	.095	.160
	Wilks' Lambda	.840	2.573[b]	2.000	27.000	.095	.160
	Hotelling's Trace	.191	2.573[b]	2.000	27.000	.095	.160
	Roy's Largest Root	.191	2.573[b]	2.000	27.000	.095	.160
Time * Genotype	Pillai's Trace	.005	.064[b]	2.000	27.000	.938	.005
	Wilks' Lambda	.995	.064[b]	2.000	27.000	.938	.005
	Hotelling's Trace	.005	.064[b]	2.000	27.000	.938	.005
	Roy's Largest Root	.005	.064[b]	2.000	27.000	.938	.005
Time * Treatment	Pillai's Trace	.089	1.316[b]	2.000	27.000	.285	.089
	Wilks' Lambda	.911	1.316[b]	2.000	27.000	.285	.089
	Hotelling's Trace	.098	1.316[b]	2.000	27.000	.285	.089
	Roy's Largest Root	.098	1.316[b]	2.000	27.000	.285	.089
Time * Genotype * Treatment	Pillai's Trace	.507	13.902[b]	2.000	27.000	.000	.507
	Wilks' Lambda	.493	13.902[b]	2.000	27.000	.000	.507
	Hotelling's Trace	1.030	13.902[b]	2.000	27.000	.000	.507
	Roy's Largest Root	1.030	13.902[b]	2.000	27.000	.000	.507

Estimates

Measure: MEASURE_1

					95% Confidence Interval	
Genotype	Treatment	Time	Mean	Std. Error	Lower Bound	Upper Bound

WT	Calcium	1	1.174	.073	1.025	1.323
		2	1.188	.085	1.015	1.361
		3	1.144	.070	.999	1.288
	EGTA	1	.872	.068	.731	1.012
		2	1.045	.080	.882	1.208
		3	1.062	.066	.926	1.198
ASM-/-	Calcium	1	.800	.084	.628	.972
		2	.962	.098	.762	1.162
		3	1.021	.081	.854	1.187
	EGTA	1	.969	.068	.828	1.109
		2	1.009	.080	.846	1.172
		3	.897	.066	.761	1.033

Pairwise Comparisons

Measure: MEASURE_1

Treatment	Time	(I) Genotype	(J) Genotype	Mean Difference (I-J)	Std. Error	Sig.[b]	95% Confidence Interval for Difference[b]	
							Lower Bound	Upper Bound
Calcium	1	WT	ASM-/-	.375*	.111	.002	.147	.602
		ASM-/-	WT	-.375*	.111	.002	-.602	-.147
	2	WT	ASM-/-	.226	.129	.091	-.039	.490
		ASM-/-	WT	-.226	.129	.091	-.490	.039
	3	WT	ASM-/-	.123	.108	.263	-.097	.343

		ASM-/-	WT	-.123	.108	.263	-.343	.097
EGTA	1	WT	ASM-/-	-.097	.097	.326	-.295	.102
		ASM-/-	WT	.097	.097	.326	-.102	.295
	2	WT	ASM-/-	.036	.113	.750	-.194	.267
		ASM-/-	WT	-.036	.113	.750	-.267	.194
	3	WT	ASM-/-	.165	.094	.090	-.028	.357
		ASM-/-	WT	-.165	.094	.090	-.357	.028

Pairwise Comparisons

Measure: MEASURE_1

Genotype	Time	(I) Treatment	(J) Treatment	Mean Difference (I-J)	Std. Error	Sig.[b]	95% Confidence Interval for Difference[b]	
							Lower Bound	Upper Bound
WT	1	Calcium	EGTA	.302*	.100	.005	.098	.507
		EGTA	Calcium	-.302*	.100	.005	-.507	-.098
	2	Calcium	EGTA	.143	.116	.229	-.095	.381
		EGTA	Calcium	-.143	.116	.229	-.381	.095
	3	Calcium	EGTA	.082	.097	.406	-.117	.280
		EGTA	Calcium	-.082	.097	.406	-.280	.117
ASM-/-	1	Calcium	EGTA	-.169	.108	.130	-.391	.053
		EGTA	Calcium	.169	.108	.130	-.053	.391
	2	Calcium	EGTA	-.047	.126	.714	-.305	.211
		EGTA	Calcium	.047	.126	.714	-.211	.305

	3	Calcium	EGTA	.123	.105	.250	-.092	.338
		EGTA	Calcium	-.123	.105	.250	-.338	.092

Pairwise Comparisons

Measure: MEASURE_1

Genotype	Treatment	(I) Time	(J) Time	Mean Difference (I-J)	Std. Error	Sig.[b]	95% Confidence Interval for Difference[b]	
							Lower Bound	Upper Bound
WT	Calcium	1	2	-.014	.085	.873	-.187	.160
			3	.031	.068	.658	-.109	.171
		2	1	.014	.085	.873	-.160	.187
			3	.044	.038	.249	-.033	.121
		3	1	-.031	.068	.658	-.171	.109
			2	-.044	.038	.249	-.121	.033
	EGTA	1	2	-.173*	.080	.038	-.337	-.010
			3	-.190*	.064	.006	-.322	-.058
		2	1	.173*	.080	.038	.010	.337
			3	-.017	.035	.637	-.089	.056
		3	1	.190*	.064	.006	.058	.322
			2	.017	.035	.637	-.056	.089
ASM-/-	Calcium	1	2	-.163	.098	.107	-.363	.038
			3	-.221*	.079	.009	-.383	-.059
		2	1	.163	.098	.107	-.038	.363

		3	-.059	.043	.189	-.147	.030
	3	1	.221*	.079	.009	.059	.383
		2	.059	.043	.189	-.030	.147
EGTA	1	2	-.040	.080	.619	-.204	.123
		3	.071	.064	.278	-.061	.203
	2	1	.040	.080	.619	-.123	.204
		3	.111*	.035	.004	.039	.184
	3	1	-.071	.064	.278	-.203	.061
		2	-.111*	.035	.004	-.184	-.039

Three-way ANOVA at 100Hz

Within-Subjects Factors

Measure: MEASURE_1

Time	Dependent Variable
1	BL
2	t30
3	t60

Between-Subjects Factors

		Value Label	N
Genotype	1.00	WT	16
	2.00	ASM-/-	14
Treatment	1.00	Calcium	14
	2.00	EGTA	16

Descriptive Statistics

	Genotype	Treatment	Mean	Std. Deviation	N
BL	WT	Calcium	1.3126	.26487	8
		EGTA	.9641	.19329	8
		Total	1.1384	.28734	16
	ASM-/-	Calcium	.8275	.20611	6
		EGTA	1.0640	.30968	8
		Total	.9626	.28763	14
	Total	Calcium	1.1047	.34086	14

		EGTA	1.0141	.25465	16
		Total	1.0564	.29621	30
t30	WT	Calcium	1.3129	.18273	8
		EGTA	1.1751	.15691	8
		Total	1.2440	.17926	16
	ASM-/-	Calcium	1.0615	.40704	6
		EGTA	1.0733	.44130	8
		Total	1.0682	.41063	14
	Total	Calcium	1.2051	.31364	14
		EGTA	1.1242	.32425	16
		Total	1.1620	.31649	30
t60	WT	Calcium	1.2249	.22576	8
		EGTA	1.1711	.17304	8
		Total	1.1980	.19629	16
	ASM-/-	Calcium	1.1080	.29026	6
		EGTA	.9631	.38911	8
		Total	1.0252	.34564	14
	Total	Calcium	1.1748	.25190	14
		EGTA	1.0671	.31011	16
		Total	1.1174	.28490	30

Multivariate Tests[a]

Effect	Value	F	Hypothesis df	Error df	Sig.	Partial Eta Squared

Time	Pillai's Trace	.121	1.723[b]	2.000	25.000	.199	.121
	Wilks' Lambda	.879	1.723[b]	2.000	25.000	.199	.121
	Hotelling's Trace	.138	1.723[b]	2.000	25.000	.199	.121
	Roy's Largest Root	.138	1.723[b]	2.000	25.000	.199	.121
Time * Genotype	Pillai's Trace	.006	.081[b]	2.000	25.000	.923	.006
	Wilks' Lambda	.994	.081[b]	2.000	25.000	.923	.006
	Hotelling's Trace	.006	.081[b]	2.000	25.000	.923	.006
	Roy's Largest Root	.006	.081[b]	2.000	25.000	.923	.006
Time * Treatment	Pillai's Trace	.023	.296[b]	2.000	25.000	.747	.023
	Wilks' Lambda	.977	.296[b]	2.000	25.000	.747	.023
	Hotelling's Trace	.024	.296[b]	2.000	25.000	.747	.023
	Roy's Largest Root	.024	.296[b]	2.000	25.000	.747	.023
Time * Genotype * Treatment	Pillai's Trace	.405	8.511[b]	2.000	25.000	.002	.405
	Wilks' Lambda	.595	8.511[b]	2.000	25.000	.002	.405
	Hotelling's Trace	.681	8.511[b]	2.000	25.000	.002	.405
	Roy's Largest Root	.681	8.511[b]	2.000	25.000	.002	.405

Estimates

Measure: MEASURE_1

					95% Confidence Interval	
Genotype	Treatment	Time	Mean	Std. Error	Lower Bound	Upper Bound

WT	Calcium	1	1.313	.089	1.130	1.495
		2	1.313	.112	1.083	1.543
		3	1.225	.099	1.021	1.429
	EGTA	1	.964	.089	.782	1.146
		2	1.175	.112	.945	1.405
		3	1.171	.099	.967	1.375
ASM-/-	Calcium	1	.828	.102	.617	1.038
		2	1.062	.129	.796	1.327
		3	1.108	.115	.873	1.343
	EGTA	1	1.064	.089	.882	1.246
		2	1.073	.112	.844	1.303
		3	.963	.099	.759	1.167

Pairwise Comparisons

Measure: MEASURE_1

Treatment	Time	(I) Genotype	(J) Genotype	Mean Difference (I-J)	Std. Error	Sig.[b]	95% Confidence Interval for Difference[b]	
							Lower Bound	Upper Bound
Calcium	1	WT	ASM-/-	.485*	.135	.001	.207	.764
		ASM-/-	WT	-.485*	.135	.001	-.764	-.207
	2	WT	ASM-/-	.251	.171	.153	-.100	.602
		ASM-/-	WT	-.251	.171	.153	-.602	.100
	3	WT	ASM-/-	.117	.152	.448	-.195	.428
		ASM-/-	WT	-.117	.152	.448	-.428	.195

EGTA	1	WT	ASM-/-	-.100	.125	.433	-.358	.158
		ASM-/-	WT	.100	.125	.433	-.158	.358
	2	WT	ASM-/-	.102	.158	.525	-.223	.427
		ASM-/-	WT	-.102	.158	.525	-.427	.223
	3	WT	ASM-/-	.208	.140	.150	-.080	.496
		ASM-/-	WT	-.208	.140	.150	-.496	.080

Pairwise Comparisons

Measure: MEASURE_1

Genotype	Time	(I) Treatment	(J) Treatment	Mean Difference (I-J)	Std. Error	Sig.[b]	95% Confidence Interval for Difference[b]	
							Lower Bound	Upper Bound
WT	1	Calcium	EGTA	.349*	.125	.010	.091	.606
		EGTA	Calcium	-.349*	.125	.010	-.606	-.091
	2	Calcium	EGTA	.138	.158	.391	-.187	.463
		EGTA	Calcium	-.138	.158	.391	-.463	.187
	3	Calcium	EGTA	.054	.140	.705	-.235	.342
		EGTA	Calcium	-.054	.140	.705	-.342	.235
ASM-/-	1	Calcium	EGTA	-.237	.135	.093	-.515	.042
		EGTA	Calcium	.237	.135	.093	-.042	.515
	2	Calcium	EGTA	-.012	.171	.946	-.363	.339
		EGTA	Calcium	.012	.171	.946	-.339	.363
	3	Calcium	EGTA	.145	.152	.348	-.167	.456
		EGTA	Calcium	-.145	.152	.348	-.456	.167

Pairwise Comparisons

Measure: MEASURE_1

Genotype	Treatment	(I) Time	(J) Time	Mean Difference (I-J)	Std. Error	Sig.[b]	95% Confidence Interval for Difference[b]	
							Lower Bound	Upper Bound
WT	Calcium	1	2	.000	.116	.998	-.238	.238
			3	.088	.093	.356	-.104	.279
		2	1	.000	.116	.998	-.238	.238
			3	.088	.059	.148	-.033	.209
		3	1	-.088	.093	.356	-.279	.104
			2	-.088	.059	.148	-.209	.033
	EGTA	1	2	-.211	.116	.080	-.449	.027
			3	-.207*	.093	.035	-.399	-.015
		2	1	.211	.116	.080	-.027	.449
			3	.004	.059	.946	-.117	.125
		3	1	.207*	.093	.035	.015	.399
			2	-.004	.059	.946	-.125	.117
ASM-/-	Calcium	1	2	-.234	.134	.092	-.509	.041
			3	-.281*	.108	.015	-.502	-.059
		2	1	.234	.134	.092	-.041	.509
			3	-.047	.068	.501	-.187	.094
		3	1	.281*	.108	.015	.059	.502
			2	.047	.068	.501	-.094	.187

EGTA	1	2	-.009	.116	.937	-.247	.229
		3	.101	.093	.289	-.091	.293
	2	1	.009	.116	.937	-.229	.247
		3	.110	.059	.073	-.011	.231
	3	1	-.101	.093	.289	-.293	.091
		2	-.110	.059	.073	-.231	.011

Three-way ANOVA at 120Hz

Within-Subjects Factors

Measure: MEASURE_1

Time	Dependent Variable
1	BL
2	t30
3	t60

Between-Subjects Factors

		Value Label	N
Genotype	1.00	WT	16
	2.00	ASM-/-	12
Treatment	1.00	Calcium	13
	2.00	EGTA	15

Descriptive Statistics

	Genotype	Treatment	Mean	Std. Deviation	N
BL	WT	Calcium	1.3623	.21595	8
		EGTA	.9893	.20815	8
		Total	1.1758	.28122	16
	ASM-/-	Calcium	.8380	.20982	5
		EGTA	1.1266	.32632	7
		Total	1.0063	.31012	12
	Total	Calcium	1.1606	.33518	13

		EGTA	1.0533	.26894	15
		Total	1.1031	.30068	28
t30	WT	Calcium	1.3258	.21675	8
		EGTA	1.1920	.14663	8
		Total	1.2589	.19165	16
	ASM-/-	Calcium	1.1426	.41744	5
		EGTA	1.0564	.47430	7
		Total	1.0923	.43364	12
	Total	Calcium	1.2553	.30675	13
		EGTA	1.1287	.33476	15
		Total	1.1875	.32258	28
t60	WT	Calcium	1.2406	.20465	8
		EGTA	1.1771	.15238	8
		Total	1.2089	.17736	16
	ASM-/-	Calcium	1.1816	.29643	5
		EGTA	1.0106	.40815	7
		Total	1.0818	.36135	12
	Total	Calcium	1.2179	.23370	13
		EGTA	1.0994	.30067	15
		Total	1.1544	.27344	28

Multivariate Tests[a]

Effect		Value	F	Hypothesis df	Error df	Sig.	Partial Eta Squared

Time	Pillai's Trace	.120	1.564[b]	2.000	23.000	.231	.120
	Wilks' Lambda	.880	1.564[b]	2.000	23.000	.231	.120
	Hotelling's Trace	.136	1.564[b]	2.000	23.000	.231	.120
	Roy's Largest Root	.136	1.564[b]	2.000	23.000	.231	.120
Time * Genotype	Pillai's Trace	.043	.519[b]	2.000	23.000	.602	.043
	Wilks' Lambda	.957	.519[b]	2.000	23.000	.602	.043
	Hotelling's Trace	.045	.519[b]	2.000	23.000	.602	.043
	Roy's Largest Root	.045	.519[b]	2.000	23.000	.602	.043
Time * Treatment	Pillai's Trace	.021	.252[b]	2.000	23.000	.779	.021
	Wilks' Lambda	.979	.252[b]	2.000	23.000	.779	.021
	Hotelling's Trace	.022	.252[b]	2.000	23.000	.779	.021
	Roy's Largest Root	.022	.252[b]	2.000	23.000	.779	.021
Time * Genotype * Treatment	Pillai's Trace	.376	6.924[b]	2.000	23.000	.004	.376
	Wilks' Lambda	.624	6.924[b]	2.000	23.000	.004	.376
	Hotelling's Trace	.602	6.924[b]	2.000	23.000	.004	.376
	Roy's Largest Root	.602	6.924[b]	2.000	23.000	.004	.376

Estimates

Measure: MEASURE_1

					95% Confidence Interval	
Genotype	Treatment	Time	Mean	Std. Error	Lower Bound	Upper Bound

WT	Calcium	1	1.362	.087	1.183	1.541
		2	1.326	.115	1.089	1.562
		3	1.241	.097	1.040	1.441
	EGTA	1	.989	.087	.810	1.168
		2	1.192	.115	.955	1.429
		3	1.177	.097	.977	1.377
ASM-/-	Calcium	1	.838	.110	.612	1.064
		2	1.143	.145	.843	1.442
		3	1.182	.123	.928	1.435
	EGTA	1	1.127	.093	.935	1.318
		2	1.056	.123	.803	1.310
		3	1.011	.104	.797	1.225

Pairwise Comparisons

Measure: MEASURE_1

Treatment	Time	(I) Genotype	(J) Genotype	Mean Difference (I-J)	Std. Error	Sig.[b]	95% Confidence Interval for Difference[b]	
							Lower Bound	Upper Bound
Calcium	1	WT	ASM-/-	.524*	.140	.001	.236	.813
		ASM-/-	WT	-.524*	.140	.001	-.813	-.236
	2	WT	ASM-/-	.183	.185	.332	-.199	.565
		ASM-/-	WT	-.183	.185	.332	-.565	.199
	3	WT	ASM-/-	.059	.156	.709	-.264	.382
		ASM-/-	WT	-.059	.156	.709	-.382	.264

EGTA	1	WT	ASM-/-	-.137	.127	.290	-.399	.125
		ASM-/-	WT	.137	.127	.290	-.125	.399
	2	WT	ASM-/-	.136	.168	.427	-.211	.482
		ASM-/-	WT	-.136	.168	.427	-.482	.211
	3	WT	ASM-/-	.167	.142	.252	-.127	.460
		ASM-/-	WT	-.167	.142	.252	-.460	.127

Pairwise Comparisons

Measure: MEASURE_1

Genotype	Time	(I) Treatment	(J) Treatment	Mean Difference (I-J)	Std. Error	Sig.[b]	95% Confidence Interval for Difference[b]	
							Lower Bound	Upper Bound
WT	1	Calcium	EGTA	.373*	.123	.006	.120	.626
		EGTA	Calcium	-.373*	.123	.006	-.626	-.120
	2	Calcium	EGTA	.134	.162	.418	-.201	.469
		EGTA	Calcium	-.134	.162	.418	-.469	.201
	3	Calcium	EGTA	.064	.137	.648	-.220	.347
		EGTA	Calcium	-.064	.137	.648	-.347	.220
ASM-/-	1	Calcium	EGTA	-.289	.144	.056	-.585	.008
		EGTA	Calcium	.289	.144	.056	-.008	.585
	2	Calcium	EGTA	.086	.190	.654	-.306	.478
		EGTA	Calcium	-.086	.190	.654	-.478	.306
	3	Calcium	EGTA	.171	.161	.298	-.161	.503
		EGTA	Calcium	-.171	.161	.298	-.503	.161

Pairwise Comparisons

Measure: MEASURE_1

Genotype	Treatment	(I) Time	(J) Time	Mean Difference (I-J)	Std. Error	Sig.[b]	95% Confidence Interval for Difference[b]	
							Lower Bound	Upper Bound
WT	Calcium	1	2	.037	.103	.725	-.175	.248
			3	.122	.095	.213	-.075	.318
		2	1	-.037	.103	.725	-.248	.175
			3	.085	.054	.128	-.026	.197
		3	1	-.122	.095	.213	-.318	.075
			2	-.085	.054	.128	-.197	.026
	EGTA	1	2	-.203	.103	.060	-.414	.009
			3	-.188	.095	.060	-.384	.008
		2	1	.203	.103	.060	-.009	.414
			3	.015	.054	.785	-.097	.126
		3	1	.188	.095	.060	-.008	.384
			2	-.015	.054	.785	-.126	.097
ASM-/-	Calcium	1	2	-.305*	.130	.027	-.572	-.037
			3	-.344*	.120	.009	-.592	-.095
		2	1	.305*	.130	.027	.037	.572
			3	-.039	.068	.573	-.180	.102
		3	1	.344*	.120	.009	.095	.592
			2	.039	.068	.573	-.102	.180

EGTA	1	2	.070	.110	.528	-.156	.296
		3	.116	.102	.265	-.094	.326
	2	1	-.070	.110	.528	-.296	.156
		3	.046	.058	.435	-.073	.165
	3	1	-.116	.102	.265	-.326	.094
		2	-.046	.058	.435	-.165	.073

Three-way ANOVA at 150Hz

Within-Subjects Factors

Measure: MEASURE_1

Time	Dependent Variable
1	BL
2	t30
3	t60

Between-Subjects Factors

		Value Label	N
Genotype	1.00	WT	16
	2.00	ASM-/-	12
Treatment	1.00	Calcium	13
	2.00	EGTA	15

Descriptive Statistics

	Genotype	Treatment	Mean	Std. Deviation	N
BL	WT	Calcium	1.3276	.29843	8
		EGTA	1.0120	.23921	8
		Total	1.1698	.30794	16
	ASM-/-	Calcium	.8636	.20588	5
		EGTA	1.1461	.33671	7
		Total	1.0284	.31372	12
	Total	Calcium	1.1492	.34827	13

		EGTA	1.0746	.28635	15
		Total	1.1092	.31282	28
t30	WT	Calcium	1.2634	.20670	8
		EGTA	1.2176	.14793	8
		Total	1.2405	.17524	16
	ASM-/-	Calcium	1.1812	.36200	5
		EGTA	1.1000	.50642	7
		Total	1.1338	.43507	12
	Total	Calcium	1.2318	.26521	13
		EGTA	1.1627	.35291	15
		Total	1.1948	.31156	28
t60	WT	Calcium	1.2740	.18348	8
		EGTA	1.2089	.18401	8
		Total	1.2414	.18067	16
	ASM-/-	Calcium	1.1684	.36029	5
		EGTA	1.0599	.42153	7
		Total	1.1051	.38373	12
	Total	Calcium	1.2334	.25645	13
		EGTA	1.1393	.31465	15
		Total	1.1830	.28783	28

Multivariate Tests[a]

Effect	Value	F	Hypothesis df	Error df	Sig.	Partial Eta Squared

Time	Pillai's Trace	.143	1.925[b]	2.000	23.000	.169	.143
	Wilks' Lambda	.857	1.925[b]	2.000	23.000	.169	.143
	Hotelling's Trace	.167	1.925[b]	2.000	23.000	.169	.143
	Roy's Largest Root	.167	1.925[b]	2.000	23.000	.169	.143
Time * Genotype	Pillai's Trace	.018	.211[b]	2.000	23.000	.811	.018
	Wilks' Lambda	.982	.211[b]	2.000	23.000	.811	.018
	Hotelling's Trace	.018	.211[b]	2.000	23.000	.811	.018
	Roy's Largest Root	.018	.211[b]	2.000	23.000	.811	.018
Time * Treatment	Pillai's Trace	.020	.233[b]	2.000	23.000	.794	.020
	Wilks' Lambda	.980	.233[b]	2.000	23.000	.794	.020
	Hotelling's Trace	.020	.233[b]	2.000	23.000	.794	.020
	Roy's Largest Root	.020	.233[b]	2.000	23.000	.794	.020
Time * Genotype * Treatment	Pillai's Trace	.305	5.051[b]	2.000	23.000	.015	.305
	Wilks' Lambda	.695	5.051[b]	2.000	23.000	.015	.305
	Hotelling's Trace	.439	5.051[b]	2.000	23.000	.015	.305
	Roy's Largest Root	.439	5.051[b]	2.000	23.000	.015	.305

Estimates

Measure: MEASURE_1

					95% Confidence Interval	
Genotype	Treatment	Time	Mean	Std. Error	Lower Bound	Upper Bound

WT	Calcium	1	1.328	.099	1.124	1.532
		2	1.263	.114	1.027	1.500
		3	1.274	.104	1.060	1.488
	EGTA	1	1.012	.099	.808	1.216
		2	1.218	.114	.981	1.454
		3	1.209	.104	.995	1.423
ASM-/-	Calcium	1	.864	.125	.606	1.122
		2	1.181	.145	.882	1.480
		3	1.168	.131	.898	1.439
	EGTA	1	1.146	.106	.928	1.364
		2	1.100	.122	.847	1.353
		3	1.060	.111	.831	1.288

Pairwise Comparisons

Measure: MEASURE_1

Treatment	Time	(I) Genotype	(J) Genotype	Mean Difference (I-J)	Std. Error	Sig.[b]	95% Confidence Interval for Difference[b]	
							Lower Bound	Upper Bound
Calcium	1	WT	ASM-/-	.464*	.159	.008	.135	.793
		ASM-/-	WT	-.464*	.159	.008	-.793	-.135
	2	WT	ASM-/-	.082	.185	.660	-.299	.463
		ASM-/-	WT	-.082	.185	.660	-.463	.299
	3	WT	ASM-/-	.106	.167	.533	-.239	.450
		ASM-/-	WT	-.106	.167	.533	-.450	.239

EGTA	1	WT	ASM-/-	-.134	.145	.363	-.433	.164
		ASM-/-	WT	.134	.145	.363	-.164	.433
	2	WT	ASM-/-	.118	.168	.489	-.228	.463
		ASM-/-	WT	-.118	.168	.489	-.463	.228
	3	WT	ASM-/-	.149	.152	.335	-.164	.462
		ASM-/-	WT	-.149	.152	.335	-.462	.164

Pairwise Comparisons

Measure: MEASURE_1

Genotype	Time	(I) Treatment	(J) Treatment	Mean Difference (I-J)	Std. Error	Sig.[b]	95% Confidence Interval for Difference[b]	
							Lower Bound	Upper Bound
WT	1	Calcium	EGTA	.316*	.140	.033	.027	.604
		EGTA	Calcium	-.316*	.140	.033	-.604	-.027
	2	Calcium	EGTA	.046	.162	.780	-.288	.380
		EGTA	Calcium	-.046	.162	.780	-.380	.288
	3	Calcium	EGTA	.065	.146	.660	-.237	.367
		EGTA	Calcium	-.065	.146	.660	-.367	.237
ASM-/-	1	Calcium	EGTA	-.283	.164	.097	-.620	.055
		EGTA	Calcium	.283	.164	.097	-.055	.620
	2	Calcium	EGTA	.081	.190	.672	-.310	.472
		EGTA	Calcium	-.081	.190	.672	-.472	.310
	3	Calcium	EGTA	.109	.171	.533	-.245	.462
		EGTA	Calcium	-.109	.171	.533	-.462	.245

Pairwise Comparisons

Measure: MEASURE_1

Genotype	Treatment	(I) Time	(J) Time	Mean Difference (I-J)	Std. Error	Sig.[b]	95% Confidence Interval for Difference[b]	
							Lower Bound	Upper Bound
WT	Calcium	1	2	.064	.096	.508	-.133	.261
			3	.054	.095	.577	-.142	.249
		2	1	-.064	.096	.508	-.261	.133
			3	-.011	.061	.862	-.136	.114
		3	1	-.054	.095	.577	-.249	.142
			2	.011	.061	.862	-.114	.136
	EGTA	1	2	-.206*	.096	.042	-.403	-.009
			3	-.197*	.095	.049	-.393	-.001
		2	1	.206*	.096	.042	.009	.403
			3	.009	.061	.886	-.116	.134
		3	1	.197*	.095	.049	.001	.393
			2	-.009	.061	.886	-.134	.116
ASM-/-	Calcium	1	2	-.318*	.121	.015	-.567	-.068
			3	-.305*	.120	.018	-.552	-.057
		2	1	.318*	.121	.015	.068	.567
			3	.013	.077	.869	-.145	.171
		3	1	.305*	.120	.018	.057	.552
			2	-.013	.077	.869	-.171	.145

EGTA	1	2	.046	.102	.655	-.165	.257
		3	.086	.101	.403	-.123	.296
	2	1	-.046	.102	.655	-.257	.165
		3	.040	.065	.541	-.094	.174
	3	1	-.086	.101	.403	-.296	.123
		2	-.040	.065	.541	-.174	.094

Bibliography

Allen, D. G. (2009). Fatigue in working muscles. *J Appl Physiol, 106*, 358-359.

Allen, D. G., Lee, J. A., & Westerblad, H. (1989). Intracellular calcium and tension during fatigue in isolated single muscle fibres from *Xenopus laevis*. *The Journal of Physiology, 415*, 433-458.

Allen, D. G., Whitehead, N. P., & Yeung, E. W. (2005). Mechanisms of stretch-induced muscle damage in normal and dystrophic muscle: Role of ionic changes. *J Physiol, 567*, 723-735.

Ashley, C. C., Mulligan, I. P., & Lea, T. J. (1991). Ca^{2+} and activation mechanisms in skeletal muscle. *Q Rev Biophys, 24*,1-73.

Baker, A. J., Kostov, K. G., Miller, R. G., & Weiner, M. W. (1993). Slow force recovery after long-duration exercise: metabolic and activation factors in muscle fatigue. *J Appl Physiol, 74*, 2294-3000.

Bansal, D., & Campbell, K. P. (2004). Dysferlin and the plasma membrane repair in muscular dystrophy. *Trends in Cell Biology, 14*, 206-213.

Barrett, J. N., & Barrett, E. F. (1978). Excitation-contraction coupling in skeletal muscle: blockade by high extracellular concentration of calcium buffers. *Science, 200*, 1270-1272.

Bianchi, C. P., & Narayan, S. (1982). Muscle fatigue and the role of transverse tubules. *Science, 215*, 295-296.

Bonaldo, P., & Sandri, M. (2013). Cellular and molecular mechanisms of muscle atrophy. *Disease Models & Mechanisms, 6*, 25-39.

Branca, D., Gugliucci, A., Bano, D., Brini, M., & Carafoli, E. (1999). Expression, partial purification and functional properties of the muscle-specific calpain isoform p94. *Eur J Biochem, 265*, 839-846.

Butler, A., He, X., Gordon, R. E., Wu, H. S., Gatt, S., & Schuchman, E. H. (2002). Reproductive pathology and sperm physiology in acid sphingomyelinase-deficient mice. *Am J Physiol, 161*, 1061-1075.

Castro-Gomes, T., Corrotte, M., Tam, C., & Andrews, N. (2015). Plasma membrane repair is regulated extracellularly by proteases released from lysosomes. *PLOS ONES, 11*, 1-26.

Corrotte, M., Almeida, P. E., Tam, C., Castro-Gomes, T., Fernandes, M. C., Millis, B. A., … & Andrews, N. (2013). Caveolae internalization repairs wounded cells and muscle fibers. *eLife, 2*, 1-30.

Chargé, S. B. P., & Rudnicki, M. A. (2004). Cellular and molecular regulation of muscle regeneration. *Physiol. Rev., 84*, 209-238.

Chin, E. R. (2005). Role of Ca^{2+}/calmodulin-dependent kinases in skeletal muscle plasticity. *J Applied Physio, 99*, 414-423.

Chin, E. R. (2010). Intracellular Ca^{2+} signaling in skeletal muscle: Decoding a complex message. *Exerc. Sport Sci. Rev., 38*(2), 76-85.

Chin, E. R., & Allen, D. G. (1995). Raised intracellular calcium can cause subsequent failure of calcium-release in mammalian skeletal-muscle. *The Journal of Physiology – London, 487,* 19-20.

Chin, E. R, & Allen, D. G. (1996). The role of elevations in intracellular [Ca^{2+}] in the development of low frequency fatigue in mouse single muscle fibres. *J Physiol, 491*, 813-824.

Chin, E. R., & Allen, D. G. (1998). The contribution of pH-dependent mechanisms to fatigue at different intensities in mammalian single muscle fibres. *The Journal of Physiology, 512,* 831-840.

Chin, E. R., Balnave, C. D., & Allen, D. G. (1997). Role of intracellular calcium and metabolites in low-frequency fatigue of mouse skeletal muscle. *Am J Physiol Physiol, 272*, C550-C559.

Chin, E. R., Chen D., Bobyk, K. D., & Mázala, D. A. G. (2014). Perturbations in intracellular Ca^{2+} handling in skeletal muscle of a mouse model of Amyotrophic Lateral Sclerosis. *Am J Physiol Cell Physiol, 307*, C1031– C1038.

Croall, D. E., & Ersfeld, K. (2007). The calpains: Modular designs and functional diversity. *Genome Biol, 8*, 218.

Curtis, B. A. (1963). Some effects of Ca-free choline-Ringer's solution on frog skeletal muscle. *J Physiol, 166*, 75-86.

Danieli-Betto, D., Germinario, E, Esposito, A., Biral, D., & Betto, R. (2000). Effects of fatigue on sarcoplasmic reticulum and myofibrillar proprieties of rat single muscle fibers. *J Appl Physiol, 89,* 891-898.

Dawson, M. J., Gadian, D. G., & Wilkie, D. R. (1980). Mechanical relaxation rate and metabolism studied in fatiguing muscle by phosphorus nuclear magnetic resonance. *J Physiol, 299,* 465-484.

Dulhunty, A. F., & Gage, P. W. (1988). Effects of extracellular calcium concentration and dihydropyridines on contraction in mammalian skeletal muscle. *Journal of Physiology, 399*, 62-80

Edwards, R. H. T., Hill, D. K., Jones, D. A., & Merton, P.A. (1977). Fatigue of long duration in human skeletal muscle after fatigue. *J Physiol, 272*, 769-778.

Endo, M. (2009). Calcium-induced calcium release in skeletal muscle. *Physiol Rev., 89*, 1153-1176.

Favero, T. G., Zable, A. C., Bowman, M. B., Thompson, A., & Abramson, J. J. (1995). Metabolic end products inhibit sarcoplasmic reticulum Ca^{2+} release and [3H]ryonadine binding. *J Appl Physiol, 78*, 1665-1672.

Fitts, R. H., Courtright, J. B., Kim, D. H., & Witzmann, F. A. (1982). Muscle fatigue with prolonged exercise: contractile and biochemical alterations. *Am J Physiol Cell Physiol, 242*, 65-73.

Fagerberg, L., Hallström, B. M., Oksvold, P., Kampf, C., Djureinovic, D., Odeberg, J., … Uhlén, M. (2014). Analysis of the human tissue-specific expression by genome-wide integration of transcriptomics and antibody-based Proteomics. *Molecular & Cellular Proteomics : MCP, 13*(2), 397–406.

Fryer, M. W., Owen, V. J., Lamb, G. D., & Stephenson, D. G. (1995). Effects of creatine phosphate and Pi on Ca^{2+} movements and tension development in rat skinned skeletal muscle fibres. *J Physiol, 482*, 123-140.

Gabandé-Rodriguez, E., Boya, P., Labrador, V., Dotti, C. G., & Ledesma, M. D. (2014). High sphingomyelin levels induce lysosomal damage and autophagy dysfunction in Niemann Pick disease type A. *Cell Death and Differentiation, 21*, 864-875.

Gailly, P., De Becker, F., Van Schoor, M., & Gillis, J. M. (2007). In situ measurements of calpain activity in isolated muscle fibres from normal and dystrophic-lacking mdx mice. *J Physiol, 582*, 1261-1275.

Garver, W. S., Francis, G. A., Jelinek, D., Shepherd, G., Flynn, J., Castro, G., … & Meaney, F. J. (2007). The National Niemann-Pick C1 disease database: Report of clinical features and health problems. *Am J Med Genet A., 143A*, 1204-1211.

Golini, L., Chouabe, C., Berthier, C., Cusimano, V., Fornaro, M., Bonvallet, R., …& Sorrentino, V. (2011). Junctophilin 1 and 2 proteins interact with the L-type Ca^{2+} channel dihydropyridine receptors (DHPRs) in skeletal muscle. *The Journal of Biological Chemistry, 286*, 43717-43725.

Goll, D. E., Shannon, J. D., Edmunds, T., Sathe, S. K., Kleese, W. C, & Nagainis, P. A. (1983). Properties and regulation of the Ca2+-dependent proteinase. In: de Bernard B, Sottocassa GL, Sandri G, Carafoli E, Taylor AN, Vanaman TC, Williams RJP, (eds) Elsevier Science Publishers. BV, Amsterdam New York, pp 19-35.

Goll, D. E., Thompson, V. F., Li, Li, H., Wei, W., & Cong, J. (2003). The calpain system. *Physiological Reviews, 83*, 731-801.

Goñi, F. M., & Alonso, A. (2002). Sphingomyelinases: Enzymoloy and membrane activity. *FEBS Letters, 531*, 38-46.

Grynkiewics, G., Poeni, M., & Tsien, R. Y. (1985). A new generation of Ca^{2+} indicators with greatly improved fluorescence properties. *Journal of Biological Chemistry, 260*, 3440-3450.

Gumbinas, M., Larsen, M., & Liu, M. H. (1975). Peripheral neuropathy in classic Niemann-Pick disease. *Neurology, 25*, 107-113.

Hill, C. A., Thompson, M. W., Ruell, P. A., Thom, J. M., & White, M. J. (2001). Sarcoplasmic reticulum function and muscle contractile character following fatiguing exercise in humans. *J Physiol, 531*, 871–878.

Holloszy, J. O. (1967). Biochemical adaptations in muscle. Effects of exercise on mitochondrial oxygen uptake and respiratory enzyme activity in skeletal muscle. *J Biol Chem, 242*, 2278-2282.

Horinouchi, K., Erlich, S., Perl, D. P., Ferlinz, K., Bisgaier, C. L., Sandhoff, K.,… & Schuchman, E. H. (1995). Acid sphingomyelinase deficient mice: A model of types A and B Niemann-Pick disease. *Nature Genetics, 10*, 288-293.

Hubal, M. J., Gordish-Dressman, H., Thompson, P. D., Price, T. B., Hoffman, E. P., Angelopoulos, T. J.,… & Clarkson, P. M. (2005). Variability in muscle size and strength gain after unilateral resistance training. *Med Sci Sports Exerc, 37*, 964-972.

Idone, V., Tam, C., Goss, J. W., Toomre, D., Pypaert, M., & Andrews, N. W. (2008). Repair of injured plasma membrane by rapid Ca^{2+}-dependent endocytosis. *J Cell Biol, 180*, 905-914.

Jenkins, R. W., Canals, D., & Hannun, Y. A. (2009). Roles and regulation of secretory and lysosomal acid sphingomyelinase. *Cell Signal, 21*, 836-846.

Jenden, D. J., & Reger, J. F. (1963). The role of resting potential changes in the contractile failure of frog sartorius muscles during calcium deprivation. *J Physiol, 169*, 889-901.

Jenkins, R. W., Canals, D., & Hannun, Y. A. (2009). Roles and regulation of secretory and lysosomal acid sphingomyelinase. *Cell Signal, 21*, 836-846.

Jimenez, A. J., Maiuri, P., Lafaurie-Janvore, J., Perez, F., & Piel, M. (2015). Laser induced wounding of the plasma membrane and methods to study the repair process. *Methods Cell Biol, 125*, 391-408.

Jones, B. J. & Roberts, D. J. (1968). The quantitative measurement of motor inco-ordination in naive mice using an accelerating rotarod. *Journal of Pharmacy and Pharmacology*, *20*, 302–304.

Kanfer, J. N., Young, O. M., Shapiro, D., & Brady, R. O. (1966). The metabolism of sphingomyelin. I. Purification and properties of a sphingomyelin-cleaving enzyme from rat liver tissue. *J Biol Chem, 241*, 1081-1084.

Kasperek, G. J., & Snider, R. D. (1989). Total and myofibrillar degradation in isolated soleus muscles after exercise. *Am J Physiol, 257*, E1-E5.

Kong, H., Jones, P. P., Koop, A., Zhang, L., Duff, H. J., & Chen, W. S. R. (2008). Caffeine induces Ca^{2+} release by reducing the threshold for luminal Ca^{2+} activation of the ryanodine receptor. *J Biochem, 414*, 441-452.

Lamb, G. D. (2009). Mechanisms of excitation-contraction uncoupling relevant to activity-induced muscle fatigue. *Appl. Physiol. Nutr. Metab., 34*, 368-372.

Lamb, G. D., Junankar, P. R., & Stephenson, D. G. (1994). Abolition of excitation-contraction coupling in skeletal muscle by raised intracellular [Ca^{2+}]. *Proceedings of the Australian Physiological and Pharmacological Society, 25*, 76.

Lamb, G. D., Junankar, P.R., & Stephenson, D.G. (1995). Raised intracellular [Ca^{2+}] abolishes excitation-contraction coupling in skeletal muscle fibres of rat and toad. *The Journal of Physiology, 489,* 349-362.

Lamb, G. D., & Cellini, M. A. (1999). High intracellular [Ca2+] alters sarcoplasmic reticulum function in skinned skeletal muscle fibres of the rat. *J Physiol, 519*, 815-827.

Lannergren, J., & Westerblad, H. (1987). The temperature dependence of isometric contractions of single, intact fibres dissected from a mouse foot muscle. *J Physiol, 390*, 285-293.

Lüttgau, H. C., & Spiecker, W. (1979). The effects of calcium deprivation upon mechanical and electrophysiological parameters in skeletal muscle fibres of the frog. J Physiol, 296, 411-429.

Macauley, S. L., Sidman, R. L., & Schuchman, E. H. (2008). Neuropathology of the acid sphingomyelinase knockout mouse model of Niemann-Pick A disease including structure–function studies associated with cerebellar Purkinje cell degeneration. *Experimental Neurology*, *214*, 181-192.

Marcuzzo, S., Zucca, I., Mastropietro, A., Kerlero de Rosbo, N., Cavalcante, P., Tartari, S., … & Bernasconi, P. (2011). Hind limb muscle atrophy precedes cerebral neuronal degeneration in G93A-SOD1 mouse model of amyotrophic lateral sclerosis: A longitudinal MRI study. *Experimental Neurology*, *231*, 30-37.

Marimuthu, K. Murton, A.J., & Greenhaff, P. L. (2011). Mechanisms regulating muscle mass during disuse atrophy and rehabilitation in humans. *J Appl Physiol, 110*, 555-560.

Mázala, D. A. G., & Chin, E.R. (2010). Effects of ex vivo denervation on intracellular Ca2+ ratios in intact mammalian single muscle fibres. *Med Sci Sports Exerc, 42*, 828-829.

Mázala, D. A. G., Grange, R. W., & Chin, E.R. (2015). The role of proteases in excitation-contraction coupling failure in muscular dystrophy. *Am J Physiol Cell Physiol, 308*, C33–C40.

McGovern, M. M., Lippa, N., Bagiella, E., Schuchman, E. H., Desnick, R., Wasserstein, M. P. (2013). Morbidity and mortality in type B Niemann-Pick disease. Genetics in Medicine, 15, 618-623.

McGovern, M. M., Wasserstein, M. P., Giugliani, R., Bembi, B., Vanier, M. T., Mengel, E., … & Cox, G. F. (2008). A prospective, cross-sectional survey study of the natural history of Niemann-Pick disease type B. *Pediatrics*, *122*, e341-e349.

McNeil ,P. L., Miyake, K., & Vogel, S. S. (2003). The endomembrane requirement for cell surface repair. *Proc Natl Acad Sci USA, 100*, 4592–4597.

Miyake, K., & McNeil, P. L. (1995). Vesicle accumulation and exocytosis at sites of plasma membrane disruption. *J Cell Biol*, *131*, 1737–1745.

Meikle, P. J., Hopwood, J. J., Clague, A. E., & Carey, W. F. (1999). Prevalence of lysosomal storage disorders. *JAMA, 281*, 249–254.

Mendelson, D. S., Wasserstein, M. P., Desnick, R. J., Glass, R., Simpson, W., … & McGovern, M. M. (2006). Type B Niemann–Pick disease: Findings at chest radiography, thin-section CT, and pulmonary function testing. *Radiology, 238*, 339–345.

Moles, A., Turrats, N., Fernández-Checa, J. C., & Mari, M. (2011). Cathepsin B overexpression due to acid sphingomyelinase ablation promotes liver fibrosis in Niemann-Pick disease. *Journal of Biological Chemistry, 287*, 1178-1188.

Murphy, R. M. (2010). Calpains, skeletal muscle function and exercise. *Clin and Exper Pharma and Physiol, 40*, 95-102.

Murphy, R. M. (2013). Ca^{2+}-dependent proteolysis of junctophilin-1 and junctophilin-2 in skeletal and cardiac muscle. *J Physiol, 591*, 719-729.

Murphy, R. M., Goodman, C. A., McKenna, M. J., Bennie, J., Leikis, M., & Lamb, G. D. (2007). Calpain-3 is autolyzed and hence activated in human skeletal muscle 24h following a single bout of eccentric exercise. *J Appl Physiol, 103*, 926-931.

Murphy, R. M., & Lamb, G. D. (2009). Endogenous calpain-3 activation is primarily governed by small increases in resting cytoplasmic Ca^{2+} and is not dependent on stretch. *J Biol Chem, 284*, 7811-7819.

Owen, V. J., Lamb, G. D., & Stephenson, D. G. (1996). Effect of low [ATP] on depolarization-induced Ca^{2+} release in skeletal muscle fibres of the toad. *J Physiol, 493*, 309-315.

Palmer, B. M., & Moore, R. L. (2000). Excitation wavelength for Fura-2 provide a linear relationship between $[Ca^{2+}]$ and fluorescence ratio. *American Journal of Cell Physiology, 279,* C1278-C1284.

Pape, P. C., Jong, D. S., Chandler, W.K., & Baylor, S.M. (1993). Effect of Fura-2 on action potential-stimulated calcium release in cut twitch fibers from frog muscle. *J Gen Physiol, 102*, 295-332.

Payne, M. A., Jimenez-Moreno, R., Wang, Z. M., Messi, M. L., & Delbono, O. (2009). Role of Ca^{2+}, membrane excitability, and Ca^{2+} stores in failing muscle contraction with aging. *Exp Gerontol, 44*(4), 261-273.

Reddy, A., Caler, E. V., & Andrews, N. W. (2001). Plasma membrane repair is mediated by Ca^{2+}-regulated exocytosis of lysosomes. Cell, 106, 157-169.

Rennie, M. J., Edwards, H. T., Krywawych, S., Davies, C. T. M., Halliday, D., Waterlow, J. C., & Millward, D. J. (1981). Effect of exercise in protein turnover in man. *Clin Sci, 6,* 627-639.

Roots, H., Ball, G., Talbot-Ponsonby, J., King, M., McBeath, K., & Ranatunga, K. W. (2009). Muscle fatigue examined at different temperatures in experiments on intact mammalian (rat) muscle fibers. *J Appl Physiol, 106,* 378-384.

Rosenblatt, D. J., Lunt, A. I., Parry, D. J., & Partridge, T. A. (1995). Culturing satellite cells from living single muscle fiber explants. *In Vitro Cell & Dev Biol. Animal, 31*(10), 773-779.

Sacchetto, R., Margreth, A., Pelosi, M., & Carafoli, E. (1996). Colocalization of the dihydropyridine receptor, the plasma membrane calcium ATPase isoform 1 and the sodium/calcium exchanger to the junctional-membrane domain of transverse tubules of rabbit skeletal muscle. *Eur J Biochem, 237,* 483-488.

Simoneau, J., & Bouchard, C. (1995). Genetic determinism of fiber type proportion in human skeletal muscle. FASEB, 9, 1091-1095.

Smith, E. L., & Schuchman, E. H. (2008). The unexpected role of acid sphingomyelinase in cell death and the pathophysiology of common diseases. *The FASEB Journal, 22,* 3419-3431.

Sturley, S. L., Patterson, M. C., Balch, W., & Liscum, L. (2004). The pathophysiology and mechanisms of NP-C disease. *Biochim Biophys Acta. 1685,* 83-87.

Switzer, R. C. (2000). Application of silver degeneration stains for neurotoxicity testing. *Toxicologic Pathology, 28,* 70-83.

Tam, C., Idone, V., Devlin, C., Fernandes, M. C., Flannery, A., He, X.,… & Andrews, N. W. (2010). Exocytosis of acid sphingomyelinase by wounded cells promotes endocytosis and plasma membrane repair. *J Cell Biol, 189,* 1027-1038.

Togo, T., Krasieva, T. B., & Steinhardt, R. A. (2000). A decrease in membrane tension precedes successful cell-membrane repair. *Mol Biol Cell, 11,* 4339–4346.

Verburg, E., Dutka, T. L., & Lamb, G. D. (2006). Long-lasting muscle fatigue: partial disruption of excitation-contraction coupling by elevated cytosolic Ca^{2+} concentration during contraction. *American Journal of Physiology - Cell Physiology, 290,* C1199-1208.

Verburg, E., Murphy, R. M., Stephenson, D. G., & Lamb, G. D. (2005). Disruption of excitation-contraction coupling and titin by endogenous Ca^{2+}-activated proteases in toad muscle fibres. *J Physiol, 564,* 775-990.

Wasserstein, M. P., Desnick, R. J., Schuchman, E. H., Hossain, S., Wallenstein, S., Lamm, C., & McGovern, M. M. (2004). The natural history of type B Niemann-Pick Disease: Results from a 10-year longitudinal study. *Pediatrics, 114,* e672-677.

Westerblad, H., & Allen, D. G. (1991). Changes in myoplasmic calcium concentration during fatigue in single mouse muscle fibres. *Journal of General Physiology, 98,* 615-635.

Westerblad, H., & Allen, D. G. (1992). Changes in intracellular pH due to repetitive stimulation of single fibres from mouse skeletal muscle. *J Physiol, 449,* 49-71.

Westerblad, H., Duty, S., & Allen, D. G. (1993). Intracellular calcium concentration during low-frequency fatigue in isolated single fibres of mouse skeletal muscle. *J Appl Physiol, 75,* 382-388.

Westerblad, H., & Lännergren, J. (1987). The use of single, intact fibres of mammalian skeletal muscle in physiological studies. *Acta Physiologica Scandinavica, 129,* 9A.

Whitehead, N.P., Yeung, E.W., & Allen, D.G. (2006). Muscle damage in mdx (dystrophic) mice: role of calcium and reactive oxygen species. *Clin. Exp. Pharmacol. Physiol, 33,* 657–662

Yeung, E. W., Balnave, C. D., Ballard, H. J., Bourreau, J.-P., & Allen, D. G. (2002). Development of T-tubular vacuoles in eccentrically damaged mouse muscle fibres. *The Journal of Physiology, 540,* 581–592.